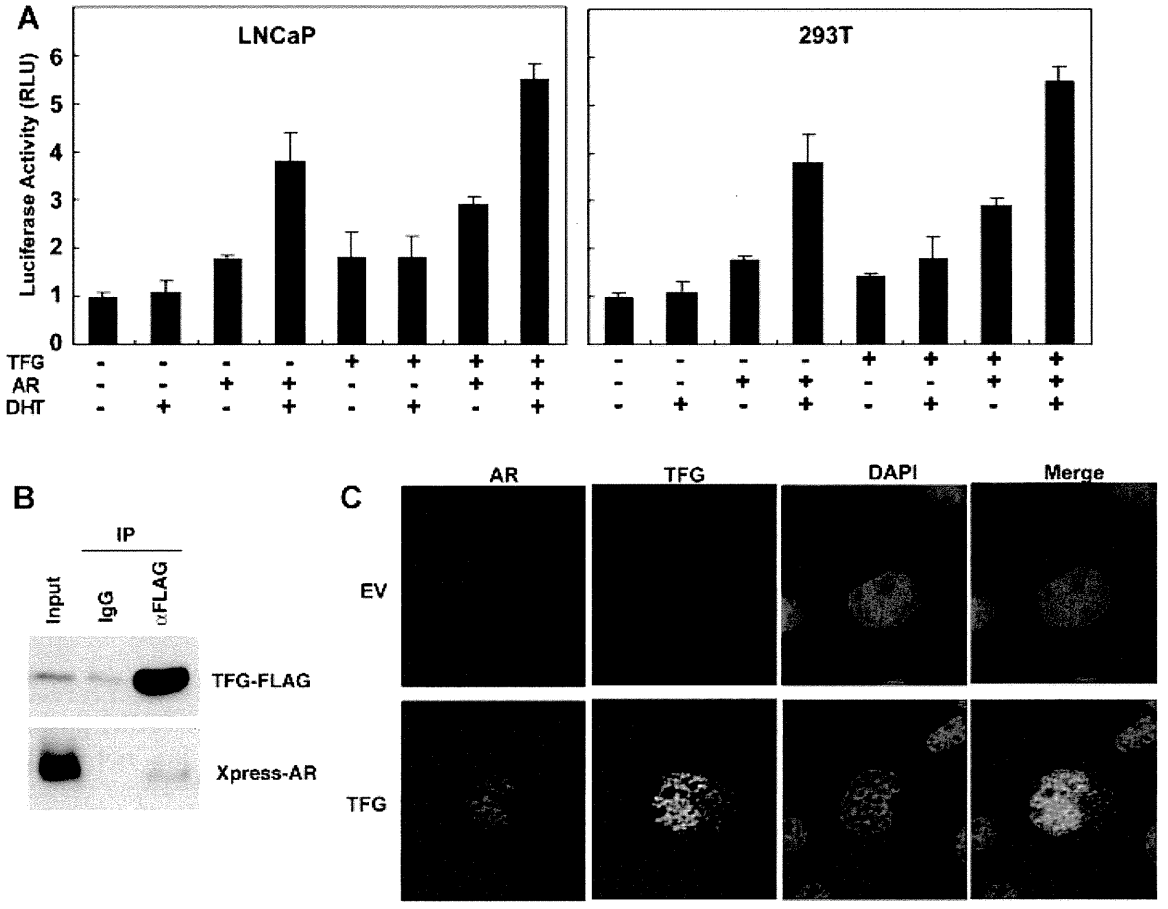

Fig. 5. Effects of TFG on prostate specific antigen (PSA) promoter activity. **A**: A luciferase reporter assay using a PSA promoter containing androgen responsive elements (AREs) was performed in LNCaP and 293T cells co-transfected with AR or TFG. Total DNA content was kept constant in all wells. Cells were treated or untreated with 10 nM dihydro-testosterone (DHT). **B**: 293T cells were co-transfected with TFG-FLAG and Xpress-AR. After 24 hr, cells were lysed and subjected to immunoprecipitation analysis with either rabbit anti-FLAG polyclonal antibody or non-immunized rabbit IgG (IgG). Immunoprecipitates were then processed for immunoblotting analysis with either anti-FLAG or anti-Xpress monoclonal antibodies. **C**: COS7 cells were transfected with Xpress-tagged AR and co-transfected with either TFG-FLAG or empty vector (EV). After 24 hr, cells were fixed and immunostained with anti-Xpress (Red) and anti-FLAG antibodies (Green) followed by confocal microscopy. Cell nuclei were counterstained with DAPI (blue).

DISCUSSION

In our present study, we demonstrate that TFG is a novel Pin1-binding phosphorylated protein in prostate cancer. TFG was found to be highly expressed in prostate cancers and its expression level was closely associated with a high tumor recurrence. Furthermore, TFG activates NF-kappaB and AR signaling and a targeted TFG depletion by specific siRNA prevents cell proliferation and induces cellular senescence in prostate cancer cells. Our current Pin1-based proteomics analysis has thus revealed that TFG could be a new potential diagnostic/prognostic marker and anti-cancer target.

Ayala et al. [22] have reported that Pin1 expression is highly correlated with a higher probability of recurrence in prostate cancer after a prostatectomy. Another report has shown that a Pin1 scoring system which sums both the nuclear and cytoplasmic grade can predict the prognosis of prostate cancer patients after a prostatectomy [23]. We have previously shown in our laboratory that Pin1 plays an important role not only in tumorigenesis but also in the maintenance of the transformed phenotype in prostate cancer cells [20]. However, Pin1 target proteins in prostate cancer have not been reported till date, and the underlying molecular mechanism has remained elusive. To address these questions, we performed Pin1-mediated proteome analyses and identified TFG as a novel Pin1 binding protein in prostate cancer cells. TFG binds Pin1 specifically in prostate cancer cells, and this interaction increases according to the degree of malignancy in Dunning rat sublines. We further found that TFG is overexpressed in prostate cancer cells or

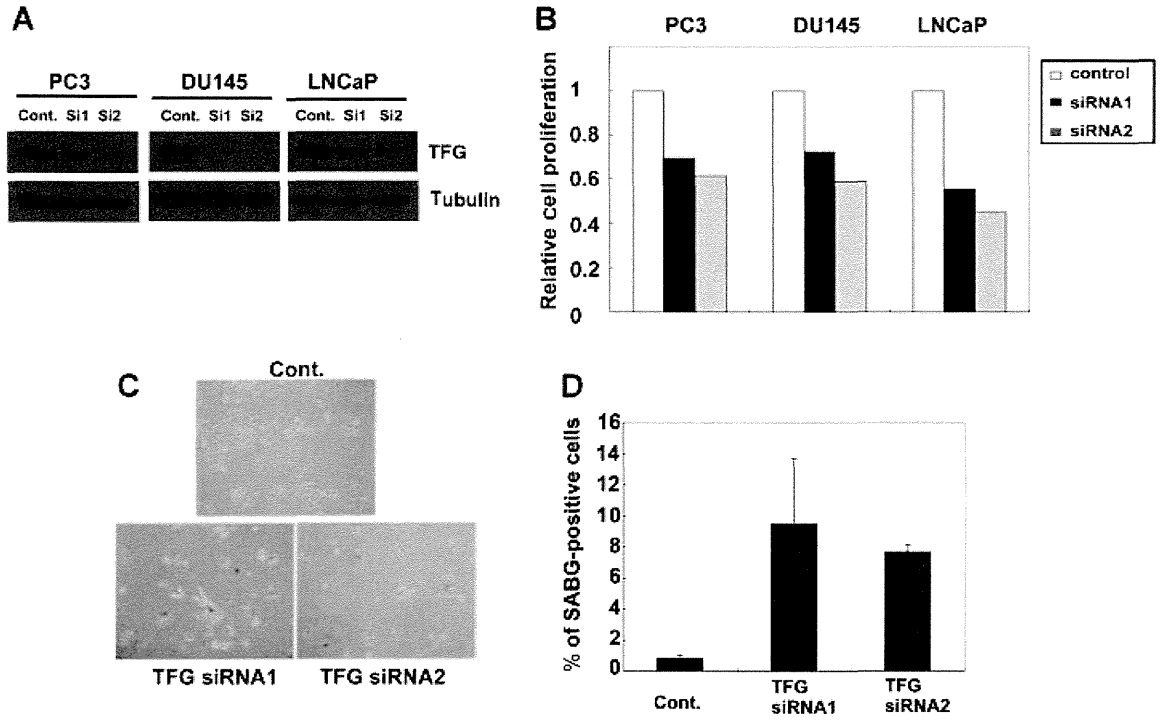

Fig. 6. TFG depletion inhibits cell growth in prostate cancer cells and induces cellular senescence. **A**, **B**: PC3, DUI45, and LNCaP cells were transduced with control-siRNA (Cont) or two different TFG siRNAs (siRNAI, siRNA2) for 96 hr. Cell lysates were extracted and then subjected to immunoblot analysis with indicated antibodies (A). Cell proliferation was assessed by the MTT assay 96 hr after siRNA transfection and the figure represents the mean of three independent experiments (B). **C**: PC3 cells transduced with the indicated siRNA were subjected to senescence-associated β-galactosidase (SABG) staining (blue). The average number of SABG–positive cells is depicted in (D).

tissues and that its inhibition results in the suppression of cell proliferation and the induction of premature senescence in these cells. In addition, Pin1 promotes TFG-mediated NF-kappaB activation by interacting with TFG on Thr206-Pro and Thr372-Pro motifs. These results indicate that Pin1 is a positive regulator of prostate cancer malignancy through TFG-mediated NF-kappaB activation.

A previous report indicates that TFG is an uncharacterized protein that associates with NEMO and TANK to enhance NF-kappaB activity [21]. TFG was shown also here to activate AR transcriptional activity suggesting that it may engage in the hormone dependency of recurrent prostate cancer. Consistent with this hypothesis, we found in our current experiments that TFG expression positively correlates with a higher rate of tumor recurrence after radical prostatectomy. These data suggest that TFG plays an important role in prostate cancer tumorigenesis by facilitating the intracellular signaling mediated by NF-kappaB and AR. Further analysis will be required to more fully characterize the collaborative actions of Pin1 and TFG during oncogenesis. Cell growth is reduced by extracellular signals including cytokines, apoptosis induction caused by DNA damage, and cell cycle arrest via cellular senescence [24,25]. We have reported previously that the suppression of Pin1 results in a substantial decrease of cell growth and the onset of specific features of senescence in prostate cancer cells [20]. In our present study, we demonstrate that the suppression of TFG results in a phenotype that is similar to when Pin1 is suppressed in prostate cancer cells.

To predict clinical outcomes in prostate cancer patients, the Gleason grade and/or PSA test are commonly used. These are standard clinicopathological parameters that can be useful in defining the clinical stage of prostate cancer. However, these parameters cannot predict the clinical outcome of prostate cancer patients with a moderate Gleason score (GS6 or GS7) [5] and a more precise predictive marker is thus desirable. Our current data suggest that TFG could be a potent and independent biomarker for recurrent prostate cancers and might therefore be a potential future therapeutic target.

CONCLUSIONS

This study reveals the potential utility of Pin1 as a molecular probe that can be used to screen prostate cancer specific phosphorylated proteins. This approach has identified TFG as a new Pin1 binding

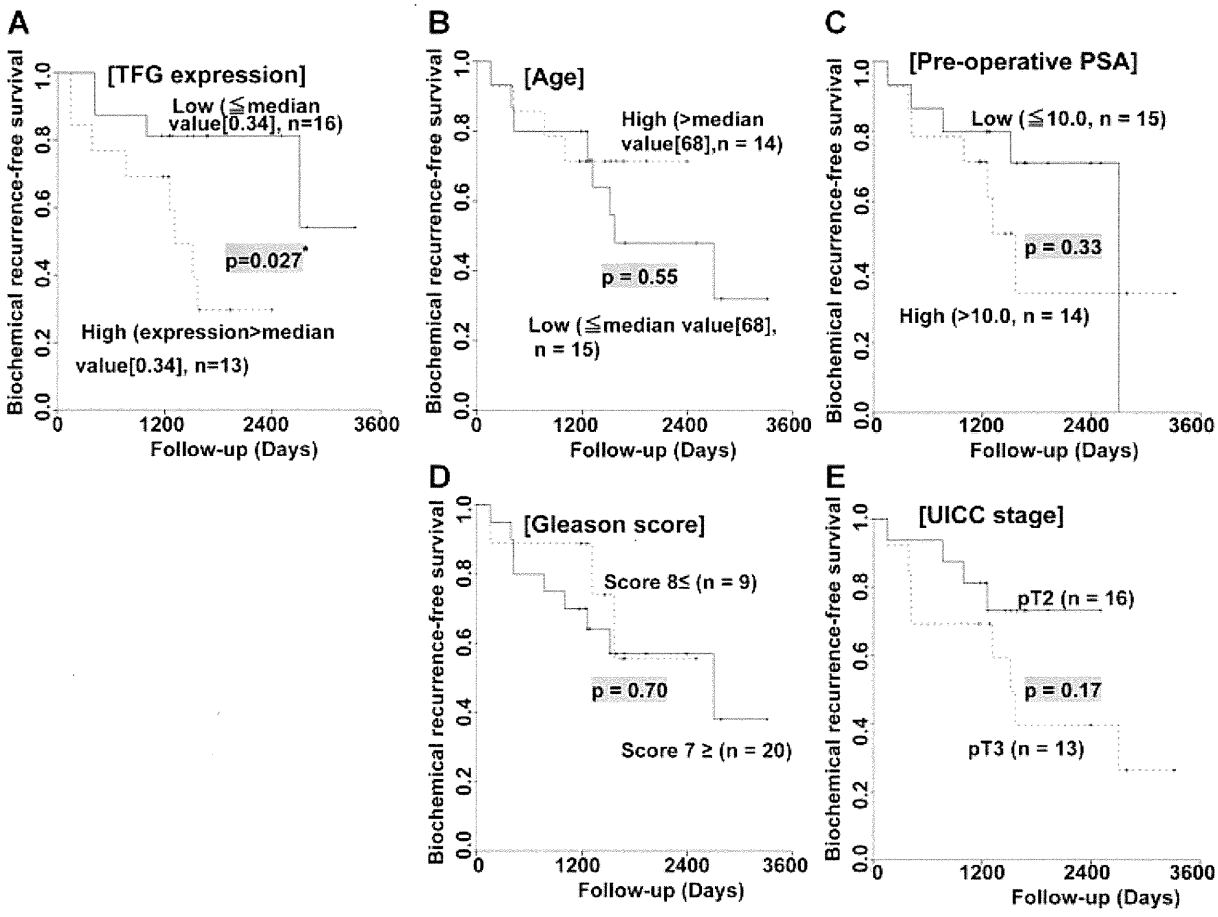

Fig. 7. Association between TFG expression and prostate cancer recurrence. **A–E**: Association of TFG expression levels (A), Age (B), Pre-operative PSA (C), Gleason score (D), or UICC stage (E) with recurrence-free survival. The Kaplan–Meier method and Log rank test were performed in prostate cancers (n = 29) with each parameter. $P \leq 0.05$ indicates statistical significance. (*: $P < 0.05$).

TABLE II. Relative Hazard of Recurrence Free Survival in Multivariate Analysis

		HR	95% CI	*P*
TFG expression				
Low expression (≦0.34)	(n = 16)			
High expression (0.34<)	(n = 13)	4.35	1.08–17.58	0.04*
Pre-operative PSA (ng/ml)				
≦10.0	(n = 15)			
10.0<	(n = 14)	1.8	0.45–7.12	0.41
Gleason score				
≦7	(n = 20)			
8≦	(n = 9)	0.53	0.11–2.56	0.43
UICC stage				
pT2	(n = 16)			
pT3	(n = 13)	1.86	0.48–7.20	0.37
Age (years)				
≦68	(n = 15)			
68<	(n = 14)	0.79	0.18–3.52	0.75

HR, hazard ratio; 95% CI, 95% confidence interval.
*: $P < 0.05$.

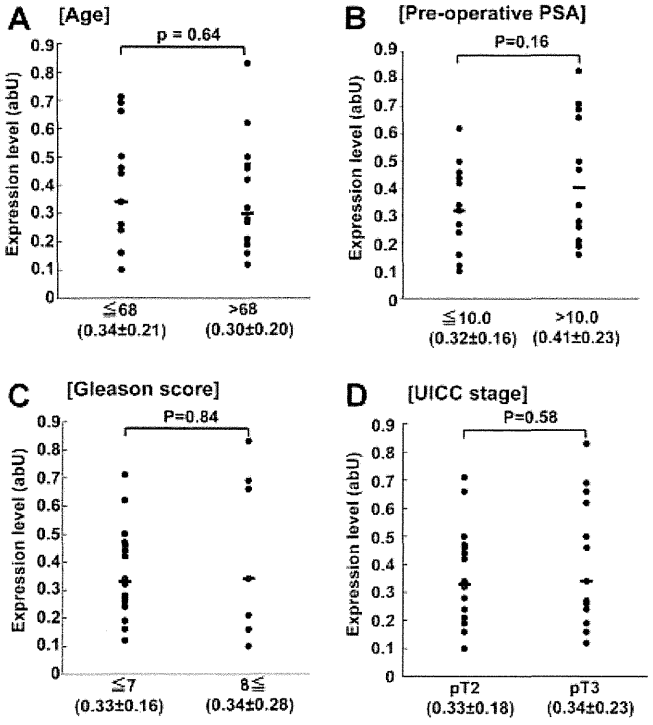

Fig. 8. Association between TFG expression and clinical parameters. **A–D**: Association of the TFG expression levels with Age (A), Pre-operative PSA (B), Gleason score (C), or UICC stage (D). Real-time quantitative PCR was carried out as described in Material and Methods section. Numerical values below columns indicate mean ± standard deviation. *P*-values were calculated by Mann–Whitney U-test. $P \leq 0.05$ indicates statistical significance.

protein in prostate cancer cell lines. TFG was shown to enhance the activity of both NF-kappaB and AR, presumably thereby contributing to prostatic oncogenesis. TFG expression shows a strong association with prostate cancer recurrence after prostatectomy. Our current data therefore indicate that TFG is a potential therapeutic target for prostate cancer and a biomarker for tumor recurrence.

ACKNOWLEDGMENTS

The authors thank T. Terada, T. Satoh (Sugiura), K. Miyoshi, and A. Kuwano for constructive advice and assistance.

REFERENCES

1. Jemal A, Siegel R, Xu J, Ward E. Cancer statistics. CA Cancer J Clin 2010;60(5):277–300.
2. Schroder FH, van der Cruijsen-Koeter I, de Koning HJ, Vis AN, Hoedemaeker RF, Kranse R. Prostate cancer detection at low prostate specific antigen. J Urol 2000;163(3):806–812.
3. Abate-Shen C, Shen MM. Molecular genetics of prostate cancer. Genes Dev 2000;14(19):2410–2434.
4. De Marzo AM, DeWeese TL, Platz EA, Meeker AK, Nakayama M, Epstein JI, Isaacs WB, Nelson WG. Pathological and molecular mechanisms of prostate carcinogenesis: Implications for diagnosis, detection, prevention, and treatment. J Cell Biochem 2004;91(3):459–477.
5. Roberts WW, Bergstralh EJ, Blute ML, Slezak JM, Carducci M, Han M, Epstein JI, Eisenberger MA, Walsh PC, Partin AW. Contemporary identification of patients at high risk of early prostate cancer recurrence after radical retropubic prostatectomy. Urology 2001;57(6):1033–1037.
6. Upreti M, Galitovskaya EN, Chu R, Tackett AJ, Terrano DT, Granell S, Chambers TC. Identification of the major phosphorylation site in Bcl-xL induced by microtubule inhibitors and analysis of its functional significance. J Biol Chem 2008; 283(51):35517–35525.
7. Kirkland PA, Humbard MA, Daniels CJ, Maupin-Furlow JA. Shotgun proteomics of the haloarchaeon Haloferax volcanii. J Proteome Res 2008;7(11):5033–5039.
8. Smal C, Vertommen D, Bertrand L, Ntamashimikiro S, Rider MH, Van Den Neste E, Bontemps F. Identification of in vivo phosphorylation sites on human deoxycytidine kinase. Role of Ser-74 in the control of enzyme activity. J Biol Chem 2006; 281(8):4887–4893.
9. Fang B, Haura EB, Smalley KS, Eschrich SA, Koomen JM. Methods for investigation of targeted kinase inhibitor therapy using chemical proteomics and phosphorylation profiling. Biochem Pharmacol 2010;80(5):739–747.
10. Kuramitsu Y, Taba K, Ryozawa S, Yoshida K, Zhang X, Tanaka T, Maehara S, Maehara Y, Sakaida I, Nakamura K. Identification of up- and down-regulated proteins in gemcitabine-resistant pancreatic cancer cells using two-dimensional gel electrophoresis and mass spectrometry. Anticancer Res 2010 30(9):3367–3372.
11. Schutkowski M, Bernhardt A, Zhou XZ, Shen M, Reimer U, Rahfeld JU, Lu KP, Fischer G. Role of phosphorylation in determining the backbone dynamics of the serine/threonine-proline motif and Pin1 substrate recognition. Biochemistry 1998; 37(16):5566–5575.
12. Ryo A, Suizu F, Yoshida Y, Perrem K, Liou YC, Wulf G, Rottapel R, Yamaoka S, Lu KP. Regulation of NF-kappaB signaling by Pin1-dependent prolyl isomerization and ubiquitin-mediated proteolysis of p65/RelA. Mol Cell 2003;12(6): 1413–1426.
13. Lam PB, Burga LN, Wu BP, Hofstatter EW, Lu KP, Wulf GM. Prolyl isomerase Pin1 is highly expressed in Her2-positive breast cancer and regulates erbB2 protein stability. Mol Cancer 2008;7:91.
14. Ryo A, Liou YC, Lu KP, Wulf G. Prolyl isomerase Pin1: A catalyst for oncogenesis and a potential therapeutic target in cancer. J Cell Sci 2003;116(Pt 5):773–783.
15. Matsuura I, Chiang KN, Lai CY, He D, Wang G, Ramkumar R, Uchida T, Ryo A, Lu K, Liu F. Pin1 promotes transforming growth factor-beta-induced migration and invasion. J Biol Chem 285(3):1754–1764.
16. Cooke DB, Quarmby VE, Petrusz P, Mickey DD, Der CJ, Isaacs JT, French FS. Expression of ras proto-oncogenes in the Dunning R3327 rat prostatic adenocarcinoma system. Prostate 1988;13(4):273–287.
17. Miyakawa K, Ryo A, Murakami T, Ohba K, Yamaoka S, Fukuda M, Guatelli J, Yamamoto N. BCA2/Rabring7 promotes tetherin-dependent HIV-1 restriction. PLoS Pathog 2009;5(12): e1000700.

18. Cookson MS, Aus G, Burnett AL, Canby-Hagino ED, D'Amico AV, Dmochowski RR, Eton DT, Forman JD, Goldenberg SL, Hernandez J, Higano CS, Kraus SR, Moul JW, Tangen C, Thrasher JB, Thompson I. Variation in the definition of biochemical recurrence in patients treated for localized prostate cancer: The American Urological Association Prostate Guidelines for Localized Prostate Cancer Update Panel report and recommendations for a standard in the reporting of surgical outcomes. J Urol 2007;177(2):540–545.
19. Greene FL, Sobin LH. A worldwide approach to the TNM staging system: Collaborative efforts of the AJCC and UICC. J Surg Oncol 2009;99(5):269–272.
20. Ryo A, Uemura H, Ishiguro H, Saitoh T, Yamaguchi A, Perrem K, Kubota Y, Lu KP, Aoki I. Stable suppression of tumorigenicity by Pin1-targeted RNA interference in prostate cancer. Clin Cancer Res 2005;11(20):7523–7531.
21. Miranda C, Roccato E, Raho G, Pagliardini S, Pierotti MA, Greco A . The TFG protein, involved in oncogenic rearrangements, interacts with TANK and NEMO, two proteins involved in the NF-kappaB pathway. J Cell Physiol 2006;208(1):154–160.
22. Ayala G, Wang D, Wulf G, Frolov A, Li R, Sowadski J, Wheeler TM, Lu KP, Bao L. The prolyl isomerase Pin1 is a novel prognostic marker in human prostate cancer. Cancer Res 2003; 63(19):6244–6251.
23. Sasaki T, Ryo A, Uemura H, Ishiguro H, Inayama Y, Yamanaka S, Kubota Y, Nagashima Y, Harada M, Aoki I. An immunohistochemical scoring system of prolyl isomerase Pin1 for predicting relapse of prostate carcinoma after radical prostatectomy. Pathol Res Pract 2006;202(5):357–364.
24. Frater-Schroder M, Risau W, Hallmann R, Gautschi P, Bohlen P. Tumor necrosis factor type alpha, a potent inhibitor of endothelial cell growth in vitro, is angiogenic in vivo. Proc Natl Acad Sci USA 1987;84(15):5277–5281.
25. Xu X, Fu XY, Plate J, Chong AS. IFN-gamma induces cell growth inhibition by Fas-mediated apoptosis: requirement of STAT1 protein for up-regulation of Fas and FasL expression. Cancer Res 1998;58(13):2832–2837.

BIOCHEMISTRY
including biophysical chemistry & molecular biology

Article

pubs.acs.org/biochemistry

N-Myristoylation of the Rpt2 Subunit Regulates Intracellular Localization of the Yeast 26S Proteasome

Ayuko Kimura,[†,‡] Yu Kato,[‡] and Hisashi Hirano*[,†,‡]

[†]Advanced Medical Research Center, Yokohama City University, Fukuura 3-9, Kanazawa, Yokohama 236-0004, Japan

[‡]Department of Supramolecular Biology, Graduate School of Nanobioscience, Yokohama City University, Suehiro 1-7-29, Tsurumi, Yokohama 230-0045, Japan

Supporting Information

ABSTRACT: The 26S proteasome is a large, complex multisubunit protease involved in protein quality control and other critical processes in eukaryotes. More than 110 post-translational modification (PTM) sites have been identified by a mass spectrometry of the 26S proteasome of *Saccharomyces cerevisiae* and are predicted to be implicated in the dynamic regulation of proteasomal functions. Here, we report that the N-myristoylation of the Rpt2 subunit controls the intracellular localization of the 26S proteasome. While proteasomes were mainly localized in the nucleus in normal cells, mutation of the N-myristoylation site of Rpt2 caused diffusion of the nuclear proteasome into the cytoplasm, where it formed aggregates. In mutant cells, the level of accumulation of cytoplasmic proteasomes was significantly increased in the nonproliferating state. Although the molecular assembly and peptidase activity of the 26S proteasome were totally unchanged in the nonmyristoylated mutants of Rpt2, an increased level of accumulation of polyubiquitinated proteins and a severe growth defect were observed in mutant cells induced for protein misfolding. In addition, polyubiquitinated protein and the nuclear protein Gcn4 tended not to colocalize with the proteasome in normal and mutant cells. Our results suggest that N-myristoylation is involved in regulating the proper intracellular distribution of proteasome activity by controlling the nuclear localization of the 26S proteasome.

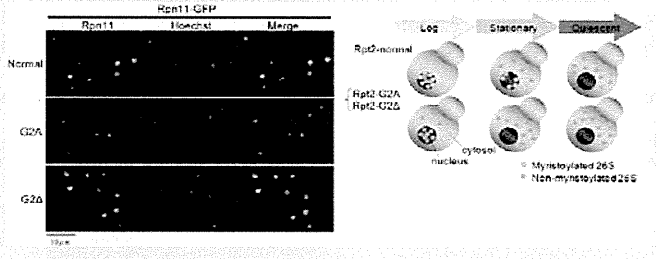

The 26S proteasome is a large multisubunit complex involved in proteolysis of polyubiquitin-tagged proteins by the ubiquitin−proteasome system (UPS), a major component in the protein quality control system. Proteins misfolded within the endoplasmic reticulum (ER) are also polyubiquitinated and exported into the cytoplasm for rapid proteasomal degradation in a process called ER-associated degradation (ERAD). In addition, various cellular processes such as the cell cycle and stress responses are under control of the UPS.[1] Tight regulation of proteins' half-lives ensures the expression of their functions at appropriate times and locations within the cell.

The 26S proteasome of eukaryotes is present in both the cytoplasm and nucleus. The functions of cytoplasmic proteasomes have been extensively analyzed; however, a growing body of evidence indicates that the nuclear proteasomes also play critical roles in the control of various nuclear functions such as gene expression, DNA repair, and nuclear protein quality control.[1] Proportions of nuclear to cytoplasmic proteasomes vary, likely depending on the cell types, culture phases, and detection methods.[1−4] The 26S proteasome is synthesized within the cytoplasm and partly imported into the nucleus through the nuclear pore complex,[5,6] whereas the active transport of proteasomes from the nucleus to the cytoplasm has not been observed. In multicellular organisms, the cytoplasmic and nuclear pools of proteasomes are separated by the nuclear envelope. Proteasomes accumulate within the nucleus during the interphase and are rapidly equilibrated by degradation of the nuclear envelope during mitosis.[7] In yeast, a unicellular organism with closed mitosis, the nuclear envelope proteins Cut8 or Sts1 tether the proteasome on the nuclear envelope, resulting in a predominantly nuclear localization of the proteasome, as has been described by many groups.[8−11] The role of the mammalian homologue of Cut8 and Sts1, which exhibits a low level of sequence similarity to yeast Cut8 and Sts1, remains unclear.[12]

The 26S proteasome consists of the 19S regulatory particle (RP) and the 20S core particle (CP). Polyubiquitinated proteins are captured by the 19S RP lid and transported into the catalytic subunit 20S CP with aid of the 19S ATPase. Thus, the degradation of polyubiquitinated proteins by the 20S CP is controlled not only by the association with the 19S RP but also by the ubiquitin binding activity and ATPase activity of the 19S RP. These activities, as well as the catalytic activity of the 20S CP itself, are predicted to be dynamically controlled by the various post-translational modifications (PTMs), as demonstrated previously in several reports.[13−16] However, there is still little direct evidence regarding the role of the particular PTM site of the proteasome.

Received: June 13, 2012
Revised: October 10, 2012
Published: October 26, 2012

Table 1. Strains and Plasmids Used in This Study

strain	relevant genotype	source
BY4741	*MAT a his3-Δ1 leu2-Δ1 ura3-Δ0 met15-Δ1*	our stock
BY4741-pRS316	*MAT a his3-Δ1 leu2-Δ1 ura3-Δ0 met15-Δ1 pRS316*	this study
α4-GFP	*MAT a his3-Δ1 leu2-Δ1 ura3-Δ0 met15-Δ1 α4::α4-GFP-hisMX6 RPT2Δ::kanMX6 RPT2/pRS316*	this study
rpn11-GFP	*MAT a his3-Δ1 leu2-Δ1 ura3-Δ0 met15-Δ1 RPN11::RPN11-GFP-His3MX6 RPT2Δ::kanMX6 RPT2/pRS316*	this study
rpn11-TEV-proA	*MAT a his3-Δ1 leu2-Δ1 ura3-Δ0 met15-Δ1 RPN11::RPN11-GFP-His3MX6 RPT2Δ::kanMX6 RPT2/pRS316*	this study
rpt2-GFP	*MAT a his3-Δ1 leu2-Δ1 ura3-Δ0 met15-Δ1 RPN11::RPN11-GFP-His3MX6 RPT2Δ::kanMX6 RPT2-GFP/ pRS315*	this study
RPT2 (normal) (α4-GFP)	*MAT a his3-Δ1 leu2-Δ1 ura3-Δ0 met15-Δ1 α4::α4-GFP-hisMX6 RPT2Δ::kanMX6 RPT2/pRS315*	this study
rpt2-G2A (α4-GFP)	*MAT a his3-Δ1 leu2-Δ1 ura3-Δ0 met15-Δ1 α4::α4-GFP-His3MX6 RPT2Δ::kanMX6 rpt2(G2A)/pRS315*	this study
rpt2-G2Δ (α4-GFP)	*MAT a his3-Δ1 leu2-Δ1 ura3-Δ0 met15-Δ1 α4::α4-GFP-His3MX6 RPT2Δ::kanMX6 rpt2(G2Δ)/pRS315*	this study
rpt2 (normal) (rpn11-GFP)	*MAT a his3-Δ1 leu2-Δ1 ura3-Δ0 met15-Δ1 RPN11::RPN11-GFP-His3MX6 RPT2Δ::kanMX6 RPT2/pRS315*	this study
rpt2-G2A (rpn11-GFP)	*MAT a his3-Δ1 leu2-Δ1 ura3-Δ0 met15-Δ1 RPN11::RPN11-GFP-His3MX6 RPT2Δ::kanMX6 rpt2(G2A)/ pRS315*	this study
rpt2-G2Δ (rpn11-GFP)	*MAT a his3-Δ1 leu2-Δ1 ura3-Δ0 met15-Δ1 RPN11::RPN11-GFP-His3MX6 RPT2Δ::kanMX6 rpt2(G2Δ)/ pRS315*	this study
rpt2 (normal) (rpn11-TEV-proA)	*MAT a his3-Δ1 leu2-Δ1 ura3-Δ0 met15-Δ1 RPN11::RPN11-TEVproA(HIS3) RPT2Δ::kanMX6 RPT2/pRS315*	this study
rpt2-G2A (rpn11-TEV-proA)	*MAT a his3-Δ1 leu2-Δ1 ura3-Δ0 met15-Δ1 RPN11::RPN11-TEVproA(HIS3) RPT2Δ::kanMX6 rpt2(G2A)/ pRS315*	this study
rpt2-G2Δ (rpn11-TEV-proA)	*MAT a his3-Δ1 leu2-Δ1 ura3-Δ0 met15-Δ1 RPN11::RPN11-TEVproA(HIS3) RPT2Δ::kanMX6 rpt2(G2Δ)/ pRS315*	this study

plasmid	composition	source
pBluescript (SK−)	*Amp* ^{r}	Agilent Technology
pFA6a-kanMX6	*pTEF Kan* ^{r} *tTEF*	27
pFA6a-His3MX6	*pTEF His5* $^{+}$ *tTEF*	27
pFA6a-GFP(S65T)-His3MX6	*GFP(S65T) tADH1 His3*	27
pRS316	*URA3 CEN6 ARSH4*	28
pRS315	*Leu2 CEN6 ARSH4*	28
pAUR123	*pADH1 tADH1 Ampr CEN4 ARS1 AUR1-C*	TAKARA
Rpt2-GFP/pRS306	*rpt2-GFP* in pRS306	this study
RPT2/pRS316	*RPT2* in pRS316	this study
RPT2/pRS315	*RPT2* in pRS315	this study
rpt2(G2A)/pRS315	*rpt2(G2A)* in pRS315	this study
rpt2(G2Δ)/pRS315	*rpt2(G2Δ)* in pRS315	this study
CFP-UBI4/pAUR123	*CFP-UBI4* in pAUR123	this study

Previously, we identified more than 110 PTM sites in the 34 subunits of the yeast 26S proteasome using mass spectrometry.[17−20] In comprehensive studies of the N-terminal peptides of the 26S proteasome, we found that the N-termini of 21 subunits are acetylated, while the N-termini of 11 subunits remained unmodified. In addition, we identified one N-myristoylation site, a relatively rare lipid modification, in the Rpt2 subunit.[19] N-Myristoylation of Rpt2 at the Gly^2 residue has also been identified in humans,[21] mice,[22] and rice[23] using mass spectrometry. The glycine residue is extensively conserved in many other eukaryotes, indicating the general importance of this modification. However, the role of the N-myristoylation of Rpt2 remains to be clarified. N-Myristoylation is an irreversible PTM in which myristic acid, a 14-carbon saturated fatty acid, is covalently attached to a glycine residue in a protein's N-terminus. It is widely accepted that *N*-myristoyl moieties mediate hydrophobic interactions with membrane lipid or other proteins and are involved in the intracellular localization or intermolecular interaction of modified proteins.[24]

Recently, the complete subunit structure of the yeast 19S RP was reported by Lander et al.[25] This structure demonstrates that the N-terminal helices of a pair of neighboring 19S ATPases, Rpt3 with Rpt6 and Rpt4 with Rpt5, form a coiled-coil protrusion, which are predicted to interact with the Rpn2 and Rpn10 subunits, respectively. In contrast, Rpt1 and Rpt2 are unlikely to participate in coiled-coil formation. The N-terminal α-helix of Rpt1 is likely to interact with the C-terminus of Rpn1, whereas there is currently no information available regarding the structural details and functions of the N-terminus of Rpt2.

To characterize the role of N-myristoylation of the Rpt2 subunit, we analyzed the molecular assembly, activity, and intracellular localization of the 26S proteasome in cells expressing nonmyristoylated mutants of Rpt2. In these mutant strains, the Gly residue at the myristoylation site has been either replaced with Ala (*rpt2*-G2A) or deleted (*rpt2*-G2Δ). A single mutation in the N-myristoylation site of Rpt2 induced the redistribution of proteasomes from the nucleus to the cytoplasm, resulting in the appearance of proteasome aggregates within the cytoplasm. This is the first report demonstrating that the PTM of a single subunit influences the intracellular localization of an entire protein complex without affecting its molecular assembly or activity.

MATERIALS AND METHODS

Yeast Strains, Plasmids, and Spot Assays. Strains and plasmids used in this study are listed in Table 1. All strains were constructed from the BY4741 strain, by inserting the GFP or TEV-protein A tag into the endogenous *RPN11*, *PRE6* (α4), or *RPT2* genes using a polymerase chain reaction (PCR)-based method.[26−28] The TEV-protein A tag, which was used for affinity purification of proteasome,[29] was inserted into the 3′-

end of the coding sequence of the endogenous RPN11 gene using a PCR-based method.[26] The rpn11-GFP and α4-GFP strains were constructed by inserting the GFP sequence into the endogenous *RPN11* and α4 genes by the same method, using a PCR fragment amplified from the pFA6a-GFP (S65T)-His3MX6 plasmid.[27] Because the deletion of the *RPT2* gene is lethal for yeast, *rpt2*-G2A and *rpt2*-G2Δ strains were constructed by plasmid shuffling. The *RPT2* (normal), *rpt2-G2A*, and *rpt2-G2Δ* genes with 1 kb of 5′ UTR sequence were subcloned into the BamHI and XhoI sites of the pRS315 or pRS316 vector.[28] The *RPT2*/pRS316 plasmid was transformed into the rpn11-GFP, α4-GFP, and rpn11-TEV-proA strains, and the rpt2-GFP/pRS316 plasmid was transformed into the rpn11-TEV-proA strain. The endogenous *RPT2* gene was substituted using the pFA6a-His3MX6 cassette[27] by homologous recombination, and positive clones were selected on SC-URA/His plates. The growth of cells was checked by the spot assay on SC-URA plates at 30 and 37 °C. Then, the *RPT2*/pRS315, *rpt2-G2A*/pRS315, and *rpt2-G2Δ*/pRS315 plasmids were transformed, and clones were selected on SC-URA/Leu plates. Plasmid shuffling was performed on SC-Leu/5′-FOA plates. For two-color imaging, a cDNA fragment containing the open reading frame of the *Saccharomyces cerevisiae UBI4* gene, N-terminally tagged with CFP, was cloned into the pAUR123 vector (Takara). The resulting vector was transformed into rpn11-GFP strains.

For the spot assay, cells precultured on SC-Leu plates were diluted to an OD_{600} of 1, spotted onto SC-Leu (or SC-Leu/Arg for canavanine) plates supplemented with the indicated reagents, and incubated for 3−5 days at 30 °C unless specified otherwise.

Sodium Dodecyl Sulfate−Polyacrylamide Gel Electrophoresis (SDS−PAGE) of Yeast Cell Lysates and Immunoblot Assay. Whole cell lysates were extracted from rpn11-TEV-proA strains by vortexing with glass beads in lysis buffer [20 mM HEPES (pH 8.0) and 9 M urea]. Polyubiquitinated proteins were detected by immunoblotting, using antibodies against mono- and polyubiquitinated conjugates (FK2H) (Enzo Life Sciences). Proteasome subunits α4 (20S) and Rpn11 (19S) were detected in the same lysates using antibodies against anti-PSMA7 (α4) (AP8659c, Abgent) and the peroxidase−antiperoxidase (PAP) soluble complex (Sigma).

Native PAGE of Yeast Cell Lysates, In-Gel Peptidase Assay, and Immunoblot Assay. Stationary cultures grown in SC-Leu medium at 30 and 37 °C were lysed by vortexing with glass beads in native lysis buffer [50 mM Tris-HCl (pH 7.5), 2 mM ATP, 5 mM $MgCl_2$, 1 mM DTT, and 1.5% (v/v) glycerol], supplemented with protease inhibitor cocktail and phosphatase inhibitor cocktail (Nacalai Tesque). After centrifugation, 30 μg of cleared lysate was loaded onto 4% native polyacrylamide gels with 0.45 mM Tris-Boric acid buffer (pH 8.3), 5 mM $MgCl_2$, 2 mM ATP, 0.5 mM EDTA, and 1 mM DTT. Electrophoresis was performed at 4 °C for 2 h at 100 V. Gels were washed in developing buffer [50 mM Tris-HCl (pH 7.4), 5 mM $MgCl_2$, and 1 mM ATP] and incubated in developing buffer containing 50 μM succinyl-Leu-Leu-Val-Tyr 4-methyl-coumaryl-7-amide [Suc-LLVY-MCA (Peptide Institute, Osaka, Japan)] for 30 min at 30 °C. Signals were detected using an ImageQuant LAS 4000-mini biomolecular imager equipped with a UV filter. Proteins in native PAGE gels were blotted onto PVDF membranes after the gels had been soaked in 1× SDS sample buffer and transfer buffer. The 26S proteasome was detected using the anti-α4 antibody.

Purification of Proteasomes, Mass Spectrometry, and Peptidase Assay. The 26S proteasome was purified from the cells expressing Rpn11-TEV-ProA as described by Kikuchi et al.,[18] using cells grown in SC-Leu medium for 72 h at 30 °C. The purified 26S proteasome was separated on a 3 to 10% gradient gel (Wako) and stained with Coomassie Brilliant Blue R-250. Each band was excised from the gel, and in-gel trypsin digestion was performed overnight at 37 °C. Peptide solutions were analyzed using MALDI-TOF/TOF-MS (4800, AB Sciex) and LC-LTQ Orbitrap (Thermo Scientific) and identified using MASCOT (Matrix Science). For peptidase assays, 2 μg of the purified proteasome was incubated with 100 μM Suc-LLVY-AMC, Ac-DEVD-MCA, or Boc-LRR-MCA (Peptide Institute) in reaction buffer [50 mM Tris-HCl (pH 7.5), 40 mM KCl, 5 mM $MgCl_2$, 0.5 mM ATP, 1 mM DTT, and 50 μg/mL BSA] at room temperature. Fluorescent signals were detected using an Infinite F200 multimode microplate reader (Tecan) equipped with a 340 nm excitation filter and a 465 nm emission filter.

Fluorescence Microscopy. Yeast cells were grown at 30 or 37 °C in 10 mL of SC-Leu medium for 5 h (log), 24 h (stationary), or 1 week (quiescent), harvested by centrifugation, and stained with 5 μL of the DNA staining dye Hoechst 33342 (Dojindo). GFP and Hoechst signals were detected in unfixed cells, using a fluorescence microscope (BZ-9000, Keyence) equipped with fluorescence filters for GFP and DAPI and a Plan Apo 100×, 1.40 oil objective lens (Nikon). ER was stained with ER stain (Subcellular Structure Localization Kit, Chemicon) and detected using a fluorescence filter appropriate for GFP. For the detection of actin, yeast cells were fixed in 4% (v/v) formaldehyde for 30 min and incubated with rhodamine-phalloidin (Subcellular Structure Localization Kit) for 2 h; these samples were observed using fluorescence filters appropriate for TRITC. For counting cells containing dotlike signals, images were obtained by overlapping the z-stack images collected at a step size of 0.2 μm. Canavanine-treated cells were streaked on SC-Leu plates with 2 μg/mL canavanine, cultured for 3 days, and harvested for observation. Quantification of the fluorescence intensity of each pixel was performed using the BZ-II image analysis application (Keyence). Photobleaching was conducted using a Zeiss LSM510 confocal microscope equipped with a C-Apochromat 63×, 1.2 Corr objective lens. A 30 mW argon laser was turned on at 75% power. For fluorescence recovery after photobleaching (FRAP) experiments, 10 iterative laser pulses at full power were applied to the nucleus or cytoplasm of the rpn11-GFP strains, and three images were collected at 30 min intervals.

Cell Fractionation. Yeast cells were grown for 24 h at 30 °C in 1 L of SC-Leu medium. The cell pellet was collected by centrifugation, and the supernatant was reused to make SC-Leu/S (2 M sorbitol in SC-Leu) medium, to avoid changing the localization pattern of the proteasome. The cell pellet was resuspended in 50 mM Tris-HCl (pH 7.5) and 30 mM DTT and incubated for 30 min at 30 °C. After centrifugation, cells were resuspended in SC-Leu/S and spheroplasted by incubation with 10 mg/mL Zymolyase 20T for 1 h at 30 °C. The pellet was resuspended and incubated for 30 min in SC-Leu/S at 30 °C and then washed twice with ice-cold SC-Leu/S and once with ice-cold 1 M sorbitol. Cells were resuspended in 6 mL of ice-cold buffer A [10 mM Tris (pH 7.5), 18% Ficoll, 20 mM potassium acetate, 5 mM magnesium acetate, 1 mM EDTA, 3 mM DTT, and protease inhibitor cocktail] and lysed

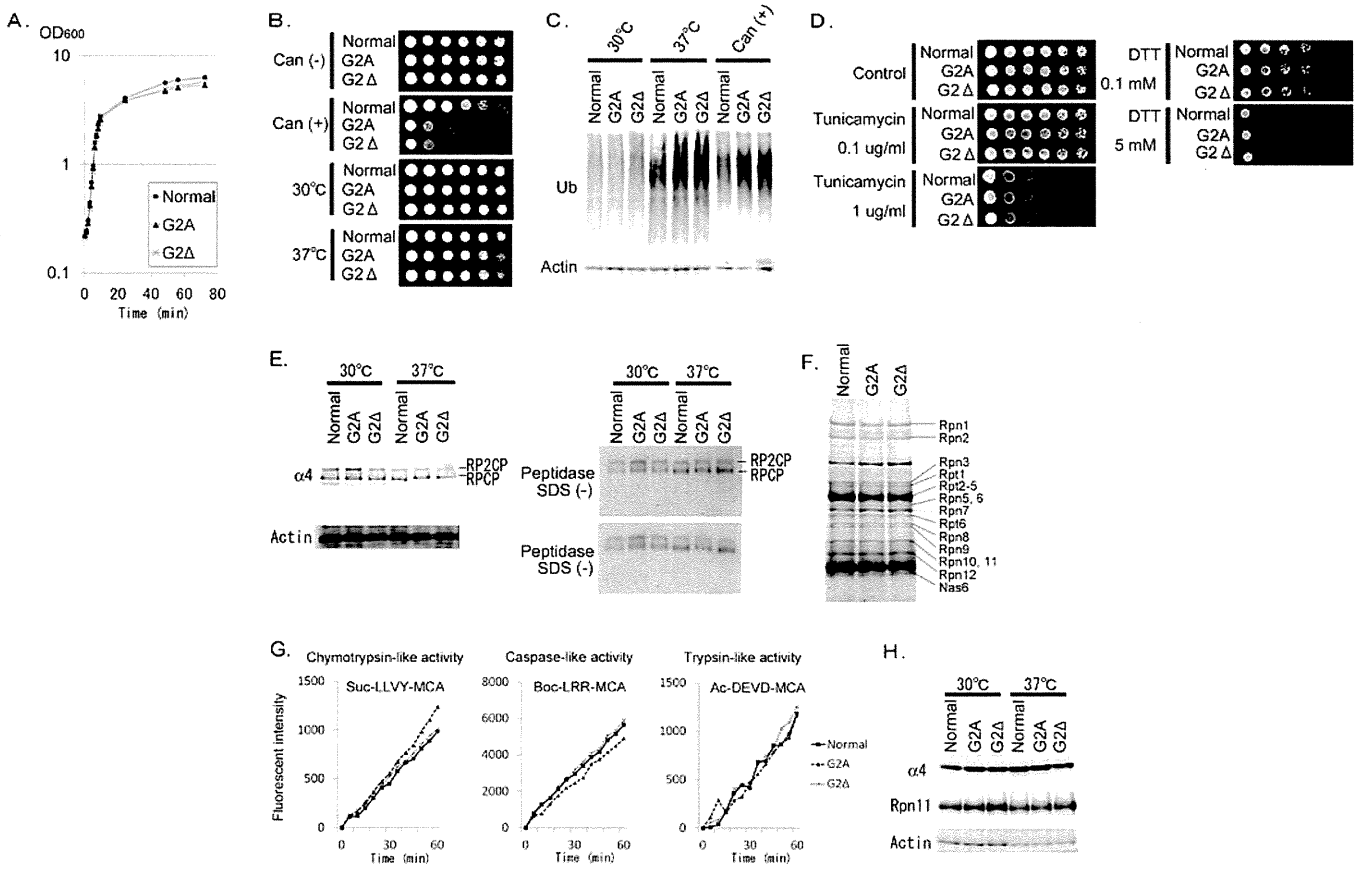

Figure 1. Phenotypes of *RPT2*, *rpt2*-G2A, and *rpt2*-G2Δ cells. (A) Growth curve. OD_{600} values of *RPT2*, *rpt2*-G2A, and *rpt2*-G2Δ cells at each time point are shown on a semilogarithmic graph. (B) Spot assay under normal and restrictive conditions. Dilutions of Rpn11-TEV-proA cells (4-fold) expressing Rpt2, Rpt2-G2A, or Rpt2-G2Δ were spotted onto SC-Leu/Arg plates with or without 2 μg/mL canavanine and incubated at 30 °C (top panels). Dilutions of the same cells (10-fold) were spotted onto SC-Leu plates and incubated at 30 or 37 °C (bottom panels). (C) Accumulation of polyubiquitinated proteins under normal or restrictive conditions. The *RPT2*, *rpt2*-G2A, and *rpt2*-G2Δ cells were cultured overnight under the indicated conditions. A total of 10 μg of yeast cell lysate was separated by SDS–PAGE and subjected to an immunoblot assay using the anti-ubiquitin antibody and anti-actin-1 antibody as a loading control. (D) Spot assay under ER stress conditions. Dilutions of cells (4-fold) were spotted onto SC-Leu plates with the indicated dilutions of tunicamycin or DTT. (E) Native PAGE of yeast cell lysate. The lysate was prepared from *RPT2*, *rpt2*-G2A, and *rpt2*-G2Δ cells grown overnight at 30 or 37 °C. A total of 30 μg of native cell lysate was subjected to native PAGE using a 4% polyacrylamide gel. The 26S proteasome was detected both by immunoblotting using the anti-α4 (20S) antibody (top left) and by the in-gel peptidase assay using suc-LLVY-AMC (right). Loaded proteins were also quantified using the anti-actin antibody (SDS–PAGE, bottom left). (F) Pull-down assay. A total of 10 μg of the purified proteasome was analyzed by SDS–PAGE and visualized using CBB staining. Each band was subjected to in-gel MS analysis. 19S subunits identified by MS/MS analysis are indicated. (G) Peptidase assay. Three peptidase activities of the proteasome (chymotrypsin-like, trypsin-like, and caspase-like activities) were analyzed using 2 μg each of proteasomes purified from *RPT2*, *rpt2*-G2A, and *rpt2*-G2Δ cells. (H) SDS–PAGE of yeast cell lysates. A total of 10 μg of lysate, prepared as described for panel C, was subjected to SDS–PAGE; α4 (20S) and Rpn11 (19S) were detected by immunoblot assays.

on ice in a Dounce homogenizer with 20 strokes of the loose pestle and 15 strokes of the tight pestle. Crude nuclei were isolated by centrifugation twice at 3500*g* for 10 min and twice at 2400*g* for 5 min. Nuclei were precipitated by centrifugation at 21600*g*, and the supernatant was collected as the cytoplasmic fraction. Fractionation was confirmed by an immunoblot assay using anti-Hsp70 (61607, BD Transduction Laboratories) and anti-Nop1 (28F2, Santa Cruz Biotechnology) antibodies, which detect cytoplasmic and nuclear markers, respectively. The 20S proteasome and Gcn4 were detected using anti-α4 and anti-Gcn4 (FL-281, Santa Cruz Biotechnology) antibodies, respectively.

RESULTS

Growth and Polyubiquitin Accumulation of *rpt2*-G2A and *rpt2*-G2Δ Mutants. Cells expressing the nonmyristoylated mutants of Rpt2, *rpt2*-G2A and *rpt2*-G2Δ, grew normally under optimal growth conditions (SC-Leu at 30 °C) (Figure 1A,B). The doubling times of normal (*RPT2*), *rpt2*-G2A, and *rpt2*-G2Δ cells were 2.09, 2.23, and 2.19 h, respectively, with a slight increase in *rpt2* mutant cells (Figure 1A). Both *rpt2*-G2A and *rpt2*-G2Δ mutants exhibited phenotypes indicating decreased proteasome activity: significant sensitivity against canavanine, an arginine analogue, and restricted growth at an elevated temperature (37 °C) (Figure 1B). Under these conditions, polyubiquitinated proteins were present at significantly higher levels in cell lysates from *rpt2*-G2A and *rpt2*-G2Δ cells than those from *RPT2* cells (Figure 1C). To confirm whether the accumulation of polyubiquitinated proteins was caused by a deficiency in ERAD, we also analyzed the effect of tunicamycin and DTT, inducers of ER stress (Figure 1D). The *rpt2*-G2A and *rpt2*-G2Δ cells exhibited no detectable ERAD deficiency, as determined by drug sensitivity.

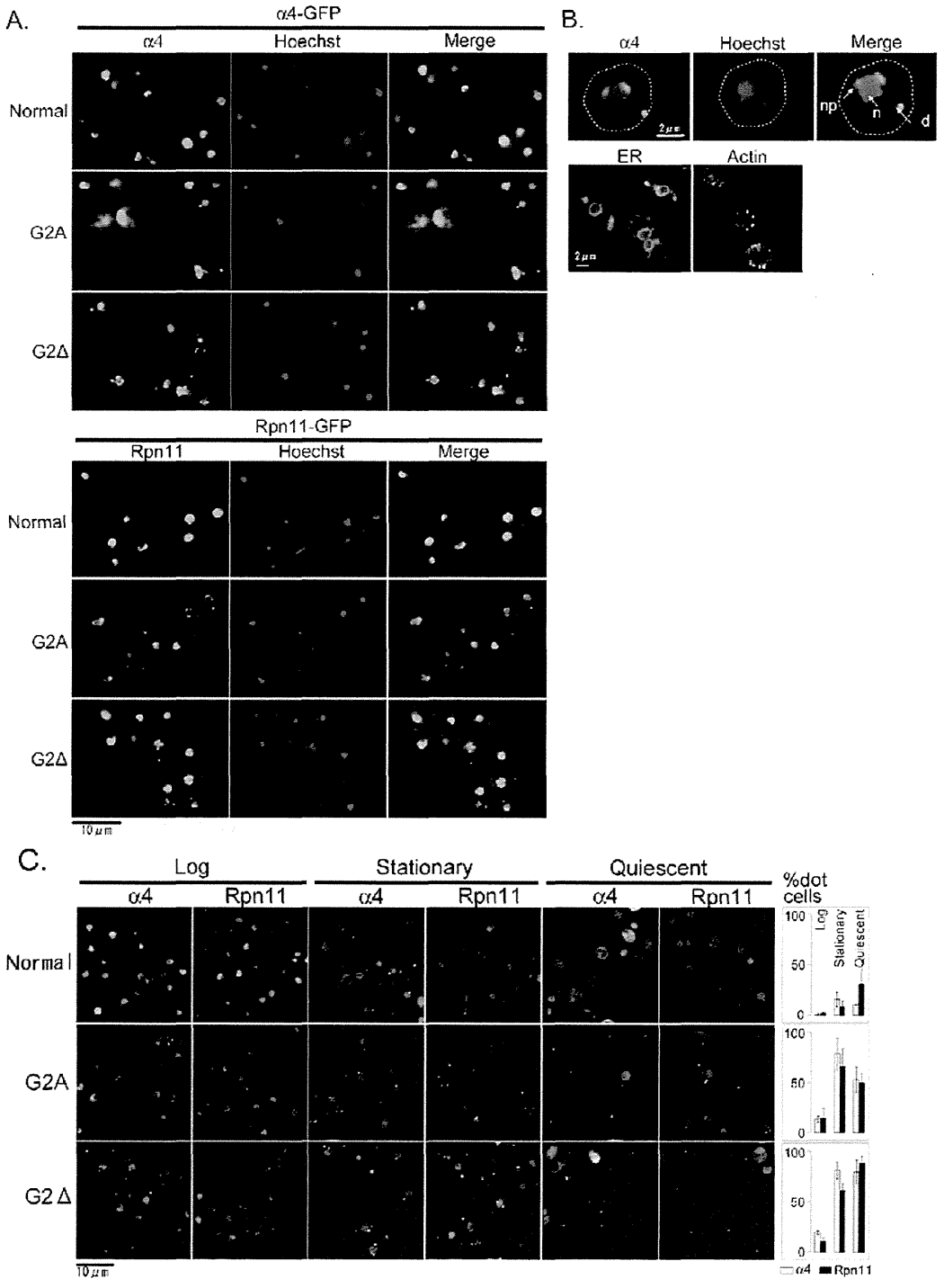

Figure 2. Intracellular localization of 26S proteasomes in *RPT2*, *rpt2*-G2A, and *rpt2*-G2Δ cells. (A) Intracellular localization of the α4 and Rpn11 subunits at log phase. α4-GFP or Rpn11-GFP was detected after incubation at 30 °C for 5 h. Typical images of the GFP and Hoechst (DNA) signals are shown. (B) Close-up of Hoechst, ER, and actin staining of the representative *rpt2*-G2A cell. Abbreviations: n, nucleus; np, nuclear periphery; d, dot. (C) Time course localization of the α4 and Rpn11 subunits. Cells cultured for 5 h (log), 1 day (stationary), or 1 week (quiescent) were used. Numbers of cells with more than one dot were counted (right graph). $n > 200$ cells for each time point (two experiments); error bars show the standard deviation.

Molecular Assembly and Peptidase Activity of the 26S Proteasome in *rpt2*-G2A and *rpt2*-G2Δ Mutants. To detect the role of N-myristoylation in the molecular assembly of the 26S proteasome, lysates of *RPT2*, *rpt2*-G2A, and *rpt2*-G2Δ cells were subjected to native PAGE followed by immunoblot detection of the 20S CP using an anti-α4 antibody (Figure 1E). The levels of 26S proteasomes, consisting of Rp_2CP and RpCP, were comparable in all strains incubated at 30 and 37 °C. The detailed subunit composition of the 19S RP was also confirmed by affinity purification of proteasomes using the TEV-proA tag inserted into the endogenous Rpn11 subunit. The SDS–PAGE pattern of the purified 19S RP was similar

dx.doi.org/10.1021/bi3007862 | *Biochemistry* 2012, 51, 8856–8866

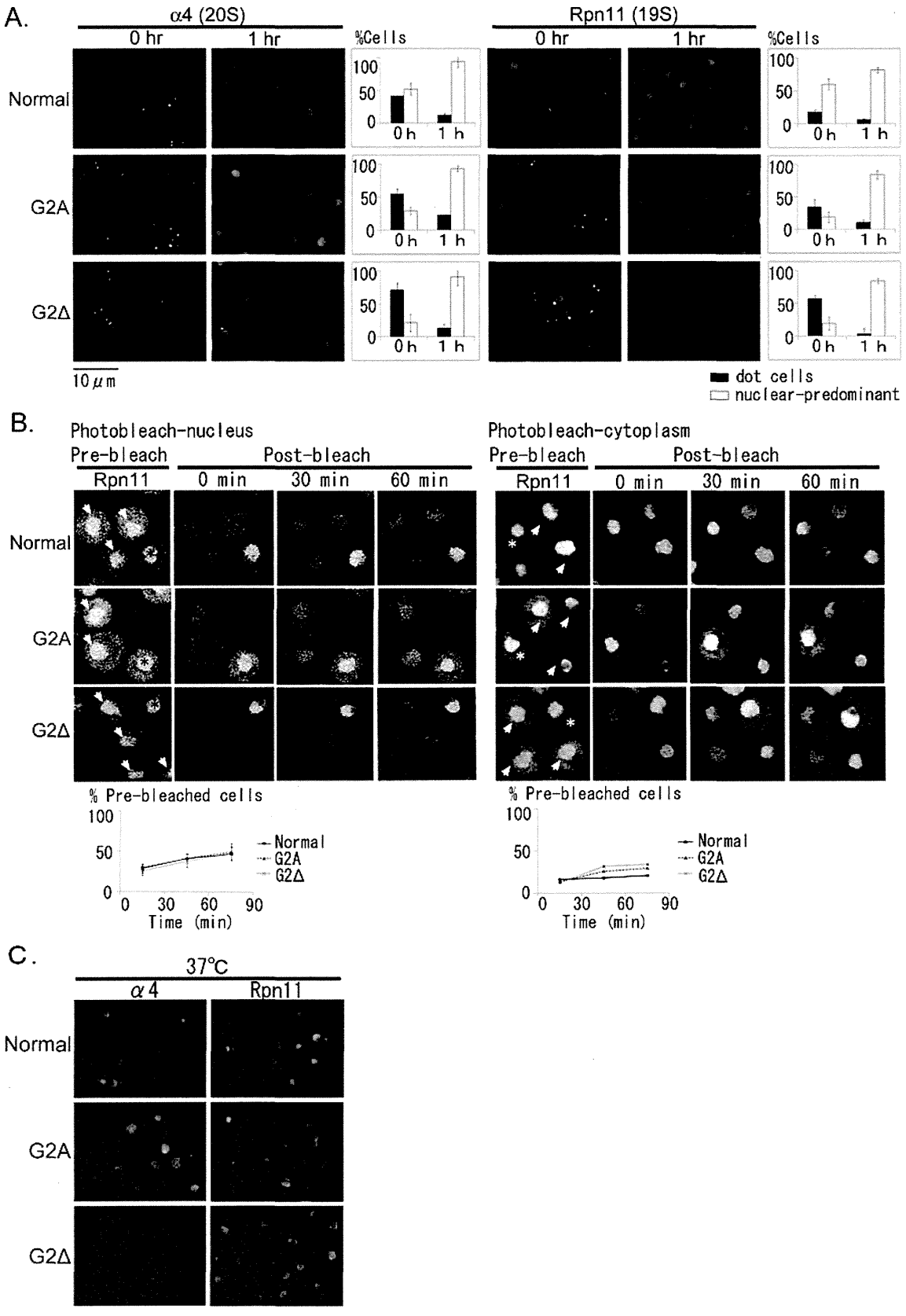

Figure 3. Intracellular localization of 26S proteasomes after medium exchange, photobleaching, or incubation at the restrictive temperature. (A) Recovery of the nuclear proteasome by medium exchange. Recovery of signals was observed in culture 0 or 1 h after the transfer of stationary phase cells into new media to induce exit from the quiescent phase. $n > 200$ cells for each time point (two experiments); error bars show the standard deviation. (B) Recovery of the nuclear and cytoplasmic proteasome after photobleaching. Using logarithmically growing rpn11-GFP cells, nuclear import of the proteasome was detected by photobleaching of the entire nucleus (left), whereas nuclear export of the proteasome was detected by photobleaching of the entire cytoplasm (right). Bleached cells are denoted with white arrows, and unbleached cells (controls) are denoted with

Figure 3. continued

asterisks. The relative signal intensity of postbleached to prebleached nucleus and cytoplasm is plotted on the graph below. (C) Intracellular localization of the 26S proteasome at the restrictive temperature. Stationary phase cultures incubated at the restrictive temperature (37 °C) were observed.

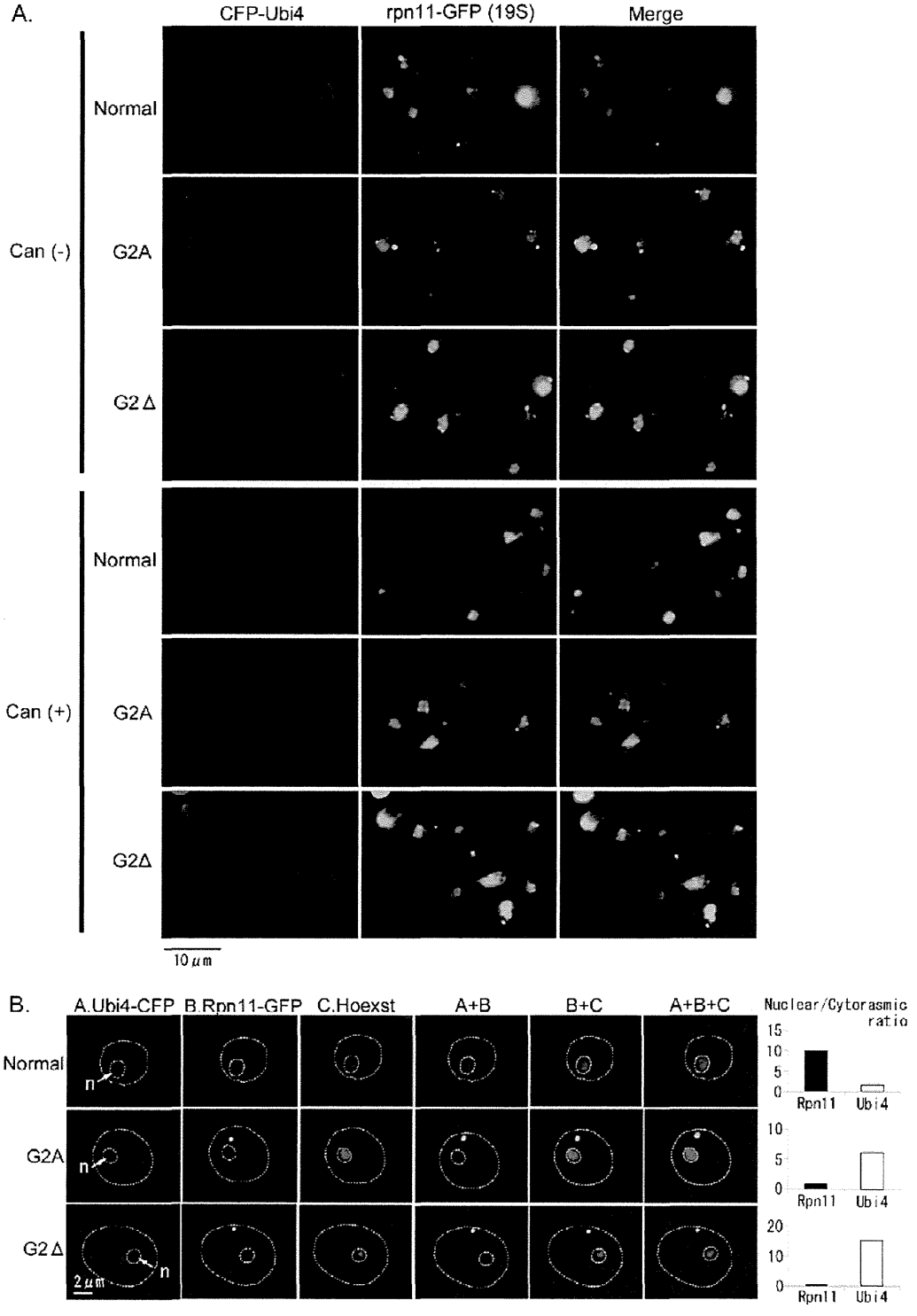

Figure 4. Intracellular localization of the polyubiquitin protein Ubi4 in *RPT2*, *rpt2*-G2A, and *rpt2*-G2Δ cells after canavanine treatment. (A) Two-color fluorescent imaging of CFP-Ubi4 (red) and Rpn11-GFP (green). Cells incubated on SC-Leu/aureobasidine plates with or without canavanine were visualized. (B) Close-up of the intracellular localization of the CFP-Ubi4 (red), Rpn11-GFP (green), and Hoechst (blue) signals in *RPT2*, *rpt2*-G2A, and *rpt2*-G2Δ cells. Cells incubated on SC-Leu/aureobasidine plates containing canavanine and stained with Hoechst 33342 were visualized. The relative signal intensity of the nucleus to cytoplasm is plotted in the graph. Nuclei are denoted with white arrows.

between *RPT2* and *rpt2* mutant cells (Figure 1F). Consistent with the data obtained by Kimura et al.,[19] both the N-myristoylated and nonmyristoylated form of Rpt2 could be detected in *RPT2* cells (Figure S1A,B of the Supporting Information). In *rpt2*-G2A and *rpt2*-G2Δ mutants, the modification of the N-terminus of Rpt2 was replaced by acetylation, a ubiquitous N-terminal modification in the 26S proteasome (Figure S1C,D of the Supporting Information).

The peptidase activity of the native 26S proteasome was analyzed by an in-gel peptidase assay using the native PAGE gels, prepared as indicated above. The chymotryptic activity of the 26S proteasome was similar between *RPT2* and *rpt2* mutant cells (Figure 1E). It has been previously reported that the deletion of three amino acid residues from the C-terminus of Rpt2 decreases the peptidase activity of the 26S proteasome, but that this activity is recovered upon treatment with 0.02% SDS (Figure 1E), which causes an artificial opening of the gate of the 20S CP.[30] In our experiment, mutation of the N-myristoylation site of Rpt2 did not change its peptidase activity regardless of the presence or absence of 0.02% SDS, indicating that the gating activity of 19S ATPase was not affected by these mutations. The chymotrypsin-like, trypsin-like, and caspase-like activities of the proteasomes purified from each strain were also comparable between the *RPT2* and *rpt2* mutant cells (Figure 1G). Finally, by immunoblot analysis of lysates prepared under denaturing conditions (9 M urea) (Figure 1H), we confirmed that the total proteasome levels were equal among these strains. Thus, we excluded the possibility that deficiencies in proteasome assembly and activity were masked by the overexpression of the proteasome, thereby compensating for the loss of functional proteasomes in mutant cells. These results indicate that the N-myristoylation of the Rpt2 subunit is not involved in the regulation of the assembly or activity of the 26S proteasome.

Intracellular Localization of the 26S Proteasome in *rpt2*-G2A and *rpt2*-G2Δ Mutants. Because the formation of the active 26S proteasome occurred normally in *rpt2*-G2A and *rpt2*-G2Δ cells, we hypothesized that N-myristoylation is involved in the regulation of its intracellular localization. To observe the in vivo localization of the 26S proteasome in the living yeast cells, we fused a GFP tag to the endogenous Rpn11 (19S) or α4 (20S) subunits (Figure S2A of the Supporting Information). Cells constitutively expressing Rpt2-GFP were not used because of their significant growth defect under optimal growth conditions (Figure S2B of the Supporting Information). In all cells, the localization patterns of α4 and Rpn11 were similar (Figure 2A), implying that the 26S complex is the predominant form of the proteasome in both *RPT2* and *rpt2* mutant cells as was also indicated in Figure 1E. Upon mutation of the N-myristoylation site of Rpt2, the localization patterns of α4-GFP and Rpn11-GFP were clearly and dramatically altered. Consistent with previous reports,[8−11] both subunits were detected mainly in the nucleus in *RPT2* cells at log phase (Figure 2A). On the other hand, in *rpt2*-G2A and *rpt2*-G2Δ mutants under the same conditions, signals in the nucleus were weakened, and bright dotlike signals appeared in the cytoplasm, showing the shift of proteasome localization from the nucleus to the cytoplasm. In some cells, the signal inside the nucleus had disappeared, whereas signals at the edge of the nucleus were retained (Figure 2B). Dotlike signals within the cytoplasm did not colocalize with mitochondria (Hoechst staining), ER, or actin (Figure 2B). In the stationary phase, dotlike signals for α4 and Rpn11 in the cytoplasm were also observed in *RPT2* cells, although they were much more prevalent in *rpt2*-G2A and *rpt2*-G2Δ mutants (Figure 2C). The number of cells with dotlike signals did not change in the stationary and quiescent (G_0) phase; however, in the quiescent phase, most signals were diffused within the cytoplasm in both *RPT2* and *rpt2* mutant cells (Figure 2C). By contrast, when *RPT2* and *rpt2*-G2A/*rpt2*-G2Δ cells were transferred to fresh medium, there was a decrease in the number of proteasome aggregates in the cytoplasm and a concomitant increase in the signal intensity of proteasomes in the nucleus, as reported by Laporte et al.[8] (Figure 3A). We also measured the nuclear import and export of proteasomes during the log phase by photobleaching the entire nuclei or cytoplasm of cells (Figure 3B). The rates of recovery of nuclear signals following photobleaching of nuclei were comparable between *RPT2* and *rpt2*-G2A/*rpt2*-G2Δ cells. In contrast, after the cytoplasm had been photobleached, signals recovered faster in *rpt2*-G2A/*rpt2*-G2Δ cells than in *RPT2* cells. Nuclear export was relatively slow compared to nuclear import, as has also been reported in *Schizosaccharomyces pombe*.[31] Taken together, these data indicate that N-myristoylation likely inhibits the leakage of nuclear proteasomes into the cytoplasm but is not involved in proteasome import.

As indicated above, the unique localization pattern of the 26S proteasome of *rpt2*-G2A and *rpt2*-G2Δ mutants was observed under normal conditions without any stress or induction of protein misfolding. Incubation of *RPT2*, *rpt2*-G2A, and *rpt2*-G2Δ cells at the restrictive temperature (37 °C) or in the presence of canavanine caused no significant changes in the localization pattern of the proteasome as compared to that of untreated cells (Figures 3C and 4A). To further confirm that the formation of proteasome aggregates is not induced by the accumulation of polyubiquitinated proteins within the cytoplasm, we ectopically expressed a CFP-tagged Ubi4 gene, which encodes a polyubiquitin protein, in the Rpn11-GFP cells, and marked sites in the cell where high levels of polyubiquitinated proteins accumulate. The CFP tag was fused at the N-terminus of the Ubi4 protein, because GFP-Ubi4 is functionally incorporated into polyubiquitin chains in HeLa cells, exhibiting localization patterns similar to those of endogenous polyubiquitin.[32] After canavanine treatment, we observed an increased level of accumulation of CFP-Ubi4 signals in large vesicle-like bodies, predominantly in the cytoplasm but also in the nucleus (Figure 4A,B). The signals for CFP-Ubi4 and Rpn11-GFP tended not to colocalize. Taken together, these data indicate that the unique localization pattern of the proteasome in cells expressing the nonmyristoylated mutant of Rpt2 was not induced by abnormal aggregation of polyubiquitinated proteins. In addition, in some *rpt2*-G2A/*rpt2*-G2Δ cells with a decreased level of the proteasome in the nucleus, the CFP-Ubi4 signals accumulated to a much greater extent in the nucleus (Figure 4B), implying that nuclear localization of the proteasome is involved in the degradation of polyubiquitinated proteins within the nucleus.

Finally, we performed cell fractionation and immunoblot assays to confirm the intracellular distribution of the 20S proteasome and the nuclear protein Gcn4, a transcriptional activator whose expression level is tightly regulated by controlled proteolysis by the proteasome (Figure 5). Efficient separation of the nuclear and cytoplasmic fractions was confirmed by immunoblot analysis using antibodies against Nop1 (nucleolar protein) and Hsp70 (cytoplasmic protein). The magnitude of the signal for α4 (20S) in the nuclear

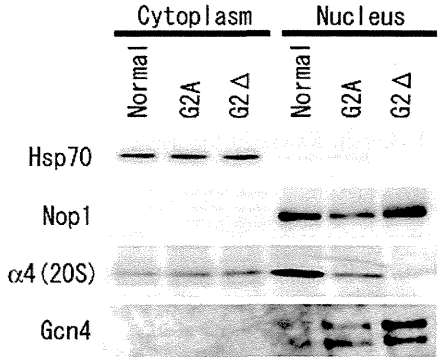

Figure 5. Cell fractionation and immunoblot analysis of the α4 and Gcn4 proteins in *RPT2*, *rpt2*-G2A, and *rpt2*-G2Δ cells. Purification of the nuclear and cytoplasmic fractions was confirmed by immunoblot assays using the antibodies against Hsp70 (cytoplasmic protein) and Nop1 (nucleolar protein). The intracellular distribution of the 20S proteasome and the nuclear protein Gcn4 was detected using anti-α4 and anti-Gcn4 antibodies, respectively.

fraction was higher in the Rpt2 cells than in the *rpt2*-G2A and *rpt2*-G2Δ cells. By contrast, the Gcn4 protein level in the nuclear fraction was higher in the mutant strains than in the normal strain, implying that N-myristoylation of Rpt2 plays a role in the degradation of nuclear proteins.

DISCUSSION

In this paper, we demonstrated that the mutation of the N-myristoylation site of Rpt2 changed the intracellular localization of the 26S proteasome without affecting its molecular assembly and activity. Strikingly, the N-myristoylation of only one subunit affects the intracellular localization of a large multi-subunit protein complex composed of more than 60 components.

N-Myristoylation is well-known to anchor proteins onto the plasma membrane,[24] but there are also some examples of a role for N-myristoylation in the nuclear anchoring of target proteins (e.g., lamin[33]). In general, N-myristoylation requires an additional force to stably anchor the target proteins onto the membrane: the hydrophobic force between another lipid moiety (e.g., palmitoyl group) and membrane lipid or the electrostatic interaction between a cluster of basic amino acids and the acidic phospholipid headgroup.[24] There is a K-rich sequence similar to a nuclear localization signal residing near the N-myristoylation site of Rpt2. Because deletion of this sequence did not affect the nuclear targeting of the 26S proteasome,[6] it is likely that N-myristoylation and the K-rich sequence function together in nuclear localization. Proteasome-activating nucleotidases (PANs), the Archaean homologues of 19S ATPases, and the N-acetylated form of 19S ATPases (Rpt3–6)[18,19] have coiled-coil protrusions formed by pairs of N-terminal helices of neighboring ATPases,[25,34] whereas coiled coils are unlikely to be formed by the Rpt1 and Rpt2 subunits, which have unmodified and myristoylated N-termini, respectively. However, on the basis of similarities with the other 19S ATPases and PANs[25,34] and the structural data regarding the 26S proteasome deposited in the EMD database (EMD-1992),[25] it is possible that the N-terminus of Rpt2 also extends outside the proteasome complex and is involved in interactions with the membrane lipid or nuclear envelope proteins (Figure 6A). The *N*-myristoyl modification of the 26S proteasome is likely to be involved in the nuclear localization of the

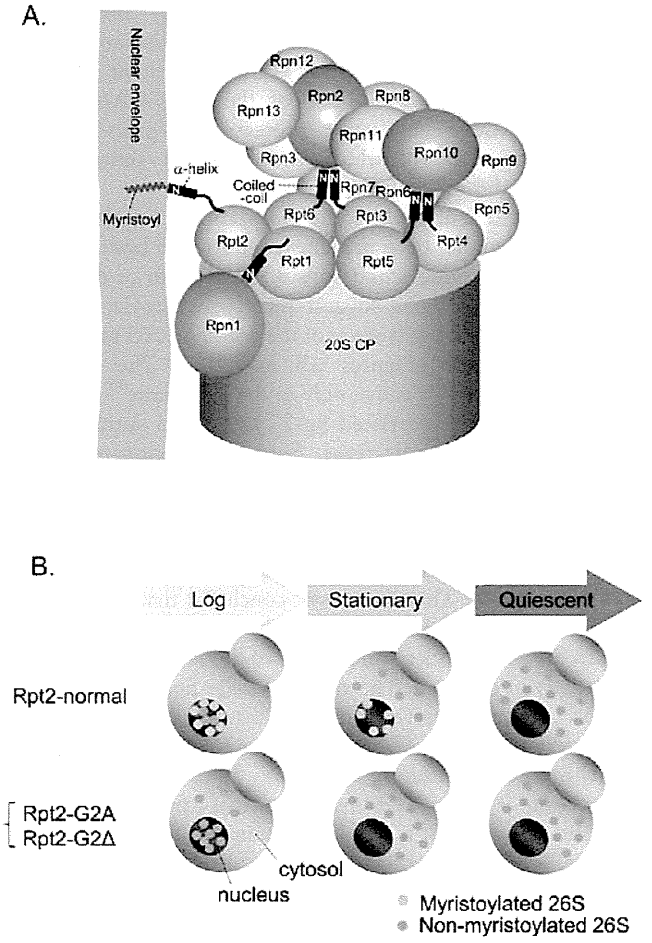

Figure 6. Schematic representation of the possible role of N-myristoylation of the Rpt2 subunit. (A) Schematic representation of the possible structures and functions of the N-terminus of each 19S ATPase. Interactions are deduced from the subunit structure revealed by Lander et al.[25] and this report. The N-terminal coiled coil formed by Rpt3 and Rpt6 likely interacts with the Rpn2 subunit, and the coiled coil formed by Rpt4 and Rpt5 is predicted to interact with the ubiquitin-interacting motif of Rpn10. The α-helices of Rpt1 and Rpt2 are unlikely to form a coiled coil. The α-helix of Rpt1 is predicted to interact with Rpn1. On the basis of similarity with the other proteasomal ATPases, the N-terminus of Rpt2 is predicted to extend outside the proteasome complex and interact with the membrane structure. (B) N-Myristoylation and nuclear localization of the 26S proteasome. During the stationary and quiescent phase, the level of N-myristoylation of the 26S proteasomes may decrease, resulting in an increase in the level of cytoplasmic aggregation of proteasomes.

proteasome via its interaction with the nuclear envelope but is probably not involved in nuclear import itself (Figure 3A,B). N-Myristoylation might also have an inhibitory effect on the formation of proteasome aggregates, which occur naturally in overgrown cells. This phenomenon is unlikely to represent aggresome formation induced by decreased proteasome activity, because no significant aggregation of polyubiquitin proteins is evident within the cytoplasm in *rpt2*-G2A or *rpt2*-G2Δ cells (Figure 4A,B). It is also possible that the aggregates, which are unlikely to be attached to any intracellular organelle or membrane structure, function as storage granules for the 26S proteasome as proposed by Laporte et al.;[8] however, to confirm this speculation, it will be necessary to isolate and functionally assay these dots. On the other hand, the previously reported nuclear tethering factor of the *S. cerevisiae* 26S proteasome,

Sts1, and N-myristoylated Rpt2 are likely involved in independent mechanisms for nuclear localization of the proteasome, because the *sts1-2* (C194Y) mutant exhibited phenotypes different from that of the *rpt2*-G2A/*rpt2*-G2Δ mutants, diffused cytoplasmic proteasome signals with no detectable aggregation, which was observed only in cells incubated at the restrictive temperature.[35]

A gradual shift of proteasome localization from the nucleus to the cytoplasm has been previously reported in both yeast and human cell lines under conditions of overgrowth or nutritional depletion.[4,8] Our results suggest that N-myristoylation might play a role in inhibiting leakage of the modified 26S proteasome from the nucleus (Figures 3B and 6B). The yeast *N*-myristoyltransferase is active only in the log phase,[36] indicating that levels of N-myristoylated Rpt2 synthesized during the log phase would slowly decrease from the stationary to the quiescent phase, because the half-life of the 26S proteasome is approximately 12−15 days.[37] In agreement with this speculation, our previous 2-DE/MS analysis revealed that only half of the 26S proteasome is N-myristoylated in the stationary phase culture.[19] Therefore, we conclude that the proper distribution of proteasomes in each phase is controlled by growth phase-dependent fluctuation of the *N*-myristoyltransferase activity in each cell. The varying localization patterns of the 26S proteasome observed among individual *RPT2* cells in the same culture might reflect heterogeneity of the growth phase and *N*-myristoyltransferase activity.

Mutation of the N-myristoylation site of Rpt2 is likely not to affect the clearance of misfolded proteins within the cytoplasm (Figure 4A). Rather, it might affect the proteasomal degradation of the minor fraction of polyubiquitinated proteins that are localized within the nucleus, as indicated in Figure 4B. The nuclear protein quality control system has been suggested to prevent the formation of insoluble protein aggregates within the nucleus under severe conditions (e.g., heat shock),[38] which might prevent normal cell growth. Accumulation of functionally critical and short-lived proteins within the nucleus, such as proteins involved in the cell cycle or gene expression [e.g., Gcn4 (Figure 5)], might have a much stronger effect on the growth of *rpt2*-G2A and *rpt2*-G2Δ cells, even if the total amount of polyubiquitinated protein is not significantly increased (Figures 1C and 5). Taken together, our results indicate that the N-myristoylation of Rpt2 is involved in the proper distribution of proteasome activity by controlling the intracellular localization of the 26S proteasome.

■ ASSOCIATED CONTENT

Ⓢ Supporting Information

Two figures. This material is available free of charge via the Internet at http://pubs.acs.org.

■ AUTHOR INFORMATION

Corresponding Author

*Telephone: 81-45-787-2791. E-mail: hirano@yokohama-cu.ac.jp.

Funding

This work was partially supported by Special Coordination Fund for Promoting Science and Technology 'Creation and Innovation Centers for Advanced Interdisciplinary'.

Notes

The authors declare no competing financial interest.

■ ACKNOWLEDGMENTS

We thank Koji Kasahara, Ken-ichi Ogura, and Nobuyuki Endo for the technical assistance with the fluorescence microscope and Kazuhiro Ogata, Masaaki Shiina, Noriaki Arakawa, Yayoi Kimura, and Hiroshi Kawasaki for useful discussions.

■ ABBREVIATIONS

PTM, post-translational modification; UPS, ubiquitin−proteasome system; ER, endoplasmic reticulum; ERAD, ER-associated degradation; RP, regulatory particle; CP, core particle; PANs, proteasome-activating nucleotidases; PAGE, polyacrylamide gel electrophoresis.

■ REFERENCES

(1) von Mikecz, A. (2006) The nuclear ubiquitin-proteasome system. *J. Cell Sci. 119*, 1977−1984.

(2) Wojcik, C., and DeMartino, G. N. (2003) Intracellular localization of proteasomes. *Int. J. Biochem. Cell Biol. 35*, 579−589.

(3) Rivett, A. J., Palmer, A., and Knecht, E. (1992) Electron microscopic localization of the multicatalytic proteinase complex in rat liver and in cultured cells. *J. Histochem. Cytochem. 40*, 1165−1172.

(4) Machiels, B. M., Henfling, M. E., Broers, J. L., Hendil, K. B., and Ramaekers, F. C. (1995) Changes in immunocytochemical detectability of proteasome epitopes depending on cell growth and fixation conditions of lung cancer cell lines. *Eur. J. Cell Biol. 66*, 282−292.

(5) Nederlof, P. M., Wang, H. R., and Baumeister, W. (1995) Nuclear localization signals of human and *Thermoplasma* proteasomal α subunits are functional in vitro. *Proc. Natl. Acad. Sci. U.S.A. 92*, 12060−12064.

(6) Wendler, P., Lehmann, A., Janek, K., Baumgart, S., and Enenkel, C. (2004) The bipartite nuclear localization sequence of Rpn2 is required for nuclear import of proteasomal base complexes via karyopherin $\alpha\beta$ and proteasome functions. *J. Biol. Chem. 279*, 37751−37762.

(7) Reits, E. A., Benham, A. M., Plougastel, B., Neefjes, J., and Trowsdale, J. (1997) Dynamics of proteasome distribution in living cells. *EMBO J. 16*, 6087−6094.

(8) Laporte, D., Salin, B., Daignan-Fornier, B., and Sagot, I. (2008) Reversible cytoplasmic localization of the proteasome in quiescent yeast cells. *J. Cell Biol. 181*, 737−745.

(9) Wilkinson, C. R., Wallace, M., Morphew, M., Perry, P., Allshire, R., Javerzat, J. P., McIntosh, J. R., and Gordon, C. (1998) Localization of the 26S proteasome during mitosis and meiosis in fission yeast. *EMBO J. 17*, 6465−6476.

(10) Enenkel, C., Lehmann, A., and Kloetzel, P. M. (1999) GFP-labelling of 26S proteasomes in living yeast: Insight into proteasomal functions at the nuclear envelope/rough ER. *Mol. Biol. Rep. 26*, 131−135.

(11) Russell, S. J., Steger, K. A., and Johnston, S. A. (1999) Subcellular localization, stoichiometry, and protein levels of 26 S proteasome subunits in yeast. *J. Biol. Chem. 274*, 21943−21952.

(12) Takeda, K., Tonthat, N. K., Glover, T., Xu, W., Koonin, E. V., Yanagida, M., and Schumacher, M. A. (2011) Implications for proteasome nuclear localization revealed by the structure of the nuclear proteasome tether protein Cut8. *Proc. Natl. Acad. Sci. U.S.A. 108*, 16950−16955.

(13) Zhang, F., Su, K., Yang, X., Bowe, D. B., Paterson, A. J., and Kudlow, J. E. (2003) O-GlcNAc modification is an endogenous inhibitor of the proteasome. *Cell 115*, 715−725.

(14) Zhang, F., Hu, Y., Huang, P., Toleman, C. A., Paterson, A. J., and Kudlow, J. E. (2007) Proteasome function is regulated by cyclic AMP-dependent protein kinase through phosphorylation of Rpt6. *J. Biol. Chem. 282*, 22460−22471.

(15) Satoh, K., Sasajima, H., Nyoumura, K. I., Yokosawa, H., and Sawada, H. (2001) Assembly of the 26S proteasome is regulated by phosphorylation of the p45/Rpt6 ATPase subunit. *Biochemistry 40*, 314−319.

(16) Bose, S., Stratford, F. L., Broadfoot, K. I., Mason, G. G., and Rivett, A. J. (2004) Phosphorylation of 20S proteasome α subunit C8 (α7) stabilizes the 26S proteasome and plays a role in the regulation of proteasome complexes by γ-interferon. *Biochem. J. 378*, 177–184.
(17) Iwafune, Y., Kawasaki, H., and Hirano, H. (2004) Identification of three phosphorylation sites in the α7 subunit of the yeast 20S proteasome in vivo using mass spectrometry. *Arch. Biochem. Biophys. 431*, 9–15.
(18) Kikuchi, J., Iwafune, Y., Akiyama, T., Okayama, A., Nakamura, H., Arakawa, N., Kimura, Y., and Hirano, H. (2010) Co- and post-translational modifications of the 26S proteasome in yeast. *Proteomics 10*, 2769–2779.
(19) Kimura, Y., Saeki, Y., Yokosawa, H., Polevoda, B., Sherman, F., and Hirano, H. (2003) N-Terminal modifications of the 19S regulatory particle subunits of the yeast proteasome. *Arch. Biochem. Biophys. 409*, 341–348.
(20) Kimura, Y., Takaoka, M., Tanaka, S., Sassa, H., Tanaka, K., Polevoda, B., Sherman, F., and Hirano, H. (2000) N(α)-acetylation and proteolytic activity of the yeast 20S proteasome. *J. Biol. Chem. 275*, 4635–4639.
(21) Wang, X., Chen, C. F., Baker, P. R., Chen, P. L., Kaiser, P., and Huang, L. (2007) Mass spectrometric characterization of the affinity-purified human 26S proteasome complex. *Biochemistry 46*, 3553–3565.
(22) Gomes, A. V., Zong, C., Edmondson, R. D., Li, X., Stefani, E., Zhang, J., Jones, R. C., Thyparambil, S., Wang, G. W., Qiao, X., Bardag-Gorce, F., and Ping, P. (2006) Mapping the murine cardiac 26S proteasome complexes. *Circ. Res. 99*, 362–371.
(23) Shibahara, T., Kawasaki, H., and Hirano, H. (2002) Identification of the 19S regulatory particle subunits from the rice 26S proteasome. *Eur. J. Biochem. 269*, 1474–1483.
(24) Resh, M. D. (1999) Fatty acylation of proteins: New insights into membrane targeting of myristoylated and palmitoylated proteins. *Biochim. Biophys. Acta 1451*, 1–16.
(25) Lander, G. C., Estrin, E., Matyskiela, M. E., Bashore, C., Nogales, E., and Martin, A. (2012) Complete subunit architecture of the proteasome regulatory particle. *Nature 482*, 186–191.
(26) Baudin, A., Ozier-Kalogeropoulos, O., Denouel, A., Lacroute, F., and Cullin, C. (1993) A simple and efficient method for direct gene deletion in *Saccharomyces cerevisiae*. *Nucleic Acids Res. 21*, 3329–3330.
(27) Longtine, M. S., McKenzie, A., III, Demarini, D. J., Shah, N. G., Wach, A., Brachat, A., Philippsen, P., and Pringle, J. R. (1998) Additional modules for versatile and economical PCR-based gene deletion and modification in *Saccharomyces cerevisiae*. *Yeast 14*, 953–961.
(28) Sikorski, R. S., and Hieter, P. (1989) A system of shuttle vectors and yeast host strains designed for efficient manipulation of DNA in *Saccharomyces cerevisiae*. *Genetics 122*, 19–27.
(29) Leggett, D. S., Glickman, M. H., and Finley, D. (2005) Purification of proteasomes, proteasome subcomplexes, and proteasome-associated proteins from budding yeast. *Methods Mol. Biol. 301*, 57–70.
(30) Smith, D. M., Chang, S. C., Park, S., Finley, D., Cheng, Y., and Goldberg, A. L. (2007) Docking of the proteasomal ATPases' carboxyl termini in the 20S proteasome's α ring opens the gate for substrate entry. *Mol. Cell 27*, 731–744.
(31) Cabrera, R., Sha, Z., Vadakkan, T. J., Otero, J., Kriegenburg, F., Hartmann-Petersen, R., Dickinson, M. E., and Chang, E. C. (2010) Proteasome nuclear import mediated by Arc3 can influence efficient DNA damage repair and mitosis in *Schizosaccharomyces pombe*. *Mol. Biol. Cell 21*, 3125–3136.
(32) Qian, S. B., Ott, D. E., Schubert, U., Bennink, J. R., and Yewdell, J. W. (2002) Fusion proteins with COOH-terminal ubiquitin are stable and maintain dual functionality in vivo. *J. Biol. Chem. 277*, 38818–38826.
(33) Prufert, K., Alsheimer, M., Benavente, R., and Krohne, G. (2005) The myristoylation site of meiotic lamin C2 promotes local nuclear membrane growth and the formation of intranuclear membranes in somatic cultured cells. *Eur. J. Cell Biol. 84*, 637–646.
(34) Zhang, F., Hu, M., Tian, G., Zhang, P., Finley, D., Jeffrey, P. D., and Shi, Y. (2009) Structural insights into the regulatory particle of the proteasome from *Methanocaldococcus jannaschii*. *Mol. Cell 34*, 473–484.
(35) Chen, L., Romero, L., Chuang, S. M., Tournier, V., Joshi, K. K., Lee, J. A., Kovvali, G., and Madura, K. (2011) Sts1 plays a key role in targeting proteasomes to the nucleus. *J. Biol. Chem. 286*, 3104–3118.
(36) Ashrafi, K., Farazi, T. A., and Gordon, J. I. (1998) A role for *Saccharomyces cerevisiae* fatty acid activation protein 4 in regulating protein N-myristoylation during entry into stationary phase. *J. Biol. Chem. 273*, 25864–25874.
(37) Tanaka, K., and Ichihara, A. (1989) Half-life of proteasomes (multiprotease complexes) in rat liver. *Biochem. Biophys. Res. Commun. 159*, 1309–1315.
(38) Chai, Y., Koppenhafer, S. L., Shoesmith, S. J., Perez, M. K., and Paulson, H. L. (1999) Evidence for proteasome involvement in polyglutamine disease: Localization to nuclear inclusions in SCA3/MJD and suppression of polyglutamine aggregation in vitro. *Hum. Mol. Genet. 8*, 673–682.

JOURNAL OF PROTEOMICS 75 (2012) 1718–1731

Available online at www.sciencedirect.com

SciVerse ScienceDirect

www.elsevier.com/locate/jprot

Effects of growth hormone on the salmon pituitary proteome

Yoichi Kurata[a], Yayoi Kimura[a], Yuko Yamanaka[a], Akiyo Ishikawa[a], Hiroyuki Okamoto[b], Tetsuji Masaoka[b], Hiroyuki Nagoya[b], Kazuo Araki[b], Shunsuke Moriyama[c], Hisashi Hirano[a,*], Tsukasa Mori[d,**]

[a]Graduate School of Nanobioscience, Yokohama City University, Suehiro 1-7-29, Tsurumi, Yokohama 230-0045, Japan
[b]Cell Engineering Section, Division of Genetics, National Research Institute of Aquaculture, Hiruta 224-1, Tamaki, Watarai, Mie 519-0423, Japan
[c]School of Marine Biosciences, Kitasato University, Kitasato 1-15-1, Sagamihara, Kanagawa 252-0373, Japan
[d]Department of Nihon University College of Bioresource Sciences, Kameino 1866, Fujisawa 252-0880, Japan

ARTICLE INFO

Article history:
Received 3 October 2011
Accepted 4 December 2011
Available online 20 December 2011

Keywords:
GH
Endocrine
Pituitary
Salmon
Proteome

ABSTRACT

Growth hormone 1 (GH1), a pituitary hormone, plays a key role in the regulation of growth. Both excess GH1 treatment and overexpression of a GH1 transgene promote growth of salmon, but these animals exhibit physiological abnormalities in viability, fertility and metabolism, which might be related to pituitary function. However, the molecular dynamics induced in the pituitary by excess GH1 remain unknown. In this study, we performed iTRAQ proteome analysis of the amago salmon pituitary, with and without excess GH1 treatment, and found that the expression levels of proteins related to endocrine systems, metabolism, cell growth and proliferation were altered in the GH1-treated pituitary. Specifically, pituitary hormone prolactin (2.29 fold), and somatolactin α (0.14 fold) changed significantly. This result was confirmed by proteome and transcriptome analyses of pituitary from the GH1-transgenic (GH1-Tg) amago salmon. The dynamics of protein and gene expression in the pituitary of GH1-Tg amago salmon were similar to those of pituitary treated with excess GH1. Our findings suggest that not only excess GH1 hormone, but also the quantitative changes in other pituitary hormones, might be essential for the abnormal growth of amago salmon. These data will be useful in future attempts to increase the productivity of fish farming.

1. Introduction

Pituitary, an endocrine organ, synthesizes and secretes various peptide hormones including growth hormone (GH), prolactin (PRL), somatolactin (SL), thyroid-stimulating hormone (TSH), luteinizing hormone (LH) and follicle-stimulating hormone (FSH) [1]. The pituitary also produces adrenocorticotropic hormone (ACTH), melanocyte-stimulating hormone (MSH) and β-endorphin, all of which are generated by proteolytic cleavage of a common pro-hormone, proopiomelanocortin (POMC) [1].

Each pituitary hormone is released into the bloodstream and each acts on different target organs in order to strictly regulate a variety of biological functions [2] such as the stress response [3], appetite [4,5] sexual maturation [2,6], thereby helping to maintain physiological homeostasis, growth and reproduction. Simultaneously, the synthesis and secretion of these hormones are controlled by hormonal feedback regulation systems [7].

Among the pituitary hormones, GH is classified into two divergent paralogs in fish, *GH1* and *GH2* [8]. GH1 has been well studied [7,10–12], though the function of GH2 is not well understood

* *Corresponding author.* Tel.: +81 45 508 7439; fax: +81 45 508 7667.
** *Corresponding author.* Tel./fax: +81 466 84 3682.
E-mail addresses: hirano@yokohama-cu.ac.jp (H. Hirano), mori.tsukasa@nihon-u.ac.jp (T. Mori).

1874-3919/$ – see front matter © 2011 Elsevier B.V. All rights reserved.
doi:10.1016/j.jprot.2011.12.009

[9]. In target tissues, GH1 binds to the GH receptor (GHR), and also acts indirectly through locally GH1-induced IGF-I production [7,10–13], in order to promote proliferation and differentiation of muscle, bone and cartilage cells. Manipulation of GH1 levels would therefore be an important potential means of increasing the productivity of fish farming [14,15].

GH1-treated/GH1 transgenic fish frequently exhibit physiological abnormalities, such as reductions of viability [16], fertility [17], and alteration of metabolism [18,19]. However, the details of the molecular dynamics in GH1-treated fish remain unknown.

In this study, we investigated the effects of excess GH1 on amago salmon pituitary. In order to identify pituitary proteins induced by excess GH1 treatment, we performed comprehensive and quantitative iTRAQ proteome analysis of the pituitary under cultured condition with and without excess GH1. In these experiments, we identified both up-regulated and down-regulated pituitary proteins involved in regulation of endocrine systems, metabolism, cell growth and proliferation. We used bioinformatic analysis to predict the phenotypes that would be affected by alterations in levels of these proteins. Furthermore, in order to confirm the relationship between excess GH1 and the regulation of proteins, we generated GH1-transgenic (GH1-Tg) amago salmon, characterized GH1-Tg phenotypes, and performed comparative quantitative proteome and transcriptome analyses of pituitary from GH1-Tg and non-transgenic (non-Tg) amago salmon. We observed that the dynamics of protein and gene expression in the pituitary of GH1-Tg amago salmon were similar to those observed in pituitary treated with excess GH1.

Based on these results, we hypothesized that not only excess GH1 hormone, but also quantitative changes in levels of the other pituitary hormones, might be important determinants of the abnormal growth of amago salmon. These findings will be important in efforts to increase the productivity of fish farming.

2. Materials and methods

2.1. *Pituitary culture for proteome analysis*

Amago salmon (*Oncorhynchus masou ishikawae*) were grown in circular tanks at 15 °C under a natural light cycle at the Fisheries Research Agency of the National Research Institute of Aquaculture in Japan. For proteome analysis, pituitaries were removed from 20 ice-anesthetized sexually immature amago salmon and immersed in ice-cold RPMI medium containing 20 mM Hepes, 9 mM sodium bicarbonate, 100 U/ml penicillin, 100 U/ml streptomycin, and 0.25 mg/ml fungizone. Next, pituitaries were incubated separately for 4 days at 12 °C in medium for organ culture [RPMI medium supplemented with 10% fetal calf serum, 100 U/ml penicillin, 100 U/ml streptomycin, and 0.25 mg/ml fungizone] with or without excess purified bovine GH1 (12.5 μg/ml, >95% pure) in order to examine the effect of excess GH1 on pituitary proteins dynamics. The method was followed by the previous report for organ culture condition of pituitary [20]. It is well known that mammalian GH1, including bovine, can bind to the fish GH1 receptor, and stimulate the growth of salmon. After culture, each pituitary was washed twice with cold PBS and homogenized in 1 ml lysis buffer [7 M urea, 2 M thiourea, 4% (w/v) CHAPS, 2% (w/v) DTT, 0.05% (w/v) SDS, and protease inhibitor cocktail] using a Polytron homogenizer (Kinematica, Bohemia, NY, USA) on ice, followed by centrifugation at 18,850 g for 30 min at 4 °C. The cleared supernatant was re-centrifuged at 69,600 g for 60 min at 4 °C. The final supernatant was stored at −80 °C until further use.

2.2. *Proteome analysis using iTRAQ reagents*

For iTRAQ labeling, the protein sample buffer was exchanged with 10 mM triethylammonium bicarbonate buffer, pH 8.5 (Sigma-Aldrich, St. Louis, MO, USA) using Microsep™ 3 k Centrifugal Devices (Pall, Port Washington, NY, USA). The protein concentration of samples was determined with a PROTEIN ASSAY kit (Bio-Rad Laboratories, Rockville, MD, USA), using bovine serum albumin as a protein standard. After cysteine blocking with methyl methanethiol sulfonate (MMTS), 32 μg of each protein sample was digested with trypsin. The resultant peptides were labeled with iTRAQ regents (AB-Sciex, Foster City, CA, USA) (Supplementary Fig. 1). After iTRAQ labeling, the samples were combined in a 1:1 ratio (v/v). Half of the combined mixtures of iTRAQ-labeled peptides were subsequently fractionated by a 2D-liquid chromatography system equipped with a strong cation exchange (SCX) column [HiQ Sil SCX, 0.5 mm inside diameter (id) × 35 mm, KYA Tech, Tokyo, Japan] in the first-dimension separation, and a reverse-phase (RP) trap column (HiQ Sil C18-3, 0.8 mm id × 3 mm, KYA Tech) in the second-dimension separation. The details of fractionation are provided in Supplementary Fig. 1. The fractionated peptides were automatically mixed with the MALDI matrix solution (4 mg/ml α-cyano-4-hydroxycinnamic acid dissolved in 80 μg/ml dibasic ammonium citrate containing 0.1% TFA and 70% acetonitrile), and directly spotted onto four ABI 4800 MALDI plates using a MALDI plate spotter (DiNa Direct Nano-flow LC system; KYA Tech). MS and MS/MS analyses of iTRAQ-labeled peptides were carried out on a MALDI-TOF/TOF mass spectrometer (4800 Proteomics Analyzer; AB-Sciex) in positive ion reflection mode using the 4000 Series Explorer Software (Ver. 3.5; AB-Sciex). The instrument laser power was set to 2800 for MS and 3600 for MS/MS acquisition. Typically, 1000 laser shots were accumulated per well, and MS spectra were acquired from 800 to 4000 Da with a minimum S/N filter of 50 for precursor ion selection. MS/MS analyses were performed for the 10 most abundant precursor ions per well, with an accumulation of 2000 shots for each spectrum. In order to look for less abundant proteins, re-interrogation of the target plates was carried out to acquire the 10 next-most intense peaks (if any were above the S/N threshold of 25). The series of total MS and MS/MS spectrum measurements was performed in duplicate, and these results were combined for data analysis.

MS and MS/MS data were analyzed using the ProteinPilot software ver 3.0 (AB-Sciex), which employs the Paragon algorithm for protein identification and relative quantitation [21]. The database (147,591 entries) consisted of amino acid sequences of fish proteins, retrieved from a subset of the NCBI non-redundant (nr) protein database (accessed April 14 2009) used for this search. The search parameters included iTRAQ labeling at N-terminus and lysine, cysteine modification by MMTS, methionine oxidation, and biological modifications predefined in the software. Other

parameters such as tryptic cleavage specificity, precursor ion mass accuracy, and fragment ion mass accuracy were set using built-in functions of the software. After protein identification, the data were further processed using the ProGroup algorithm within ProteinPilot to determine the minimal justifiable set of identified proteins. Relative abundances of proteins were calculated based on individual peptide ratios. Peptides shared among identified proteins were not included for relative quantitation. Isoform-specific relative quantitation was carried out by selecting peptides distinct to each form.

For protein identification, our criterion was the 95% confidence score cutoff (≥1.3 unused ProtScore). The *p*-value correlation analysis was calculated using the ProteinPilot software, and standard deviations were analyzed using the Statcel2 software (OMS, Saitama, Japan). In addition, we performed background noise reduction and bias correction in ProteinPilot, and then calculated the protein false discovery rate using the built-in PSPEP algorithm [22].

2.3. *Functional analysis*

For the downstream bioinformatic analysis, the differentially expressed fish protein sequences detected by proteome analysis were first searched against the human protein database (15,381 entries, NCBI nr, accessed April 14 2009) using the NCBI BLASTP program set to find homologous sequences. For the functional analysis, we used Ingenuity Pathways Analysis [(IPA), Ingenuity Systems, www.ingenuity.com] equipped with the Ingenuity Pathways Knowledge Base. By IPA, the assigned proteins were classified according to subcellular localization, molecular functions, and biological functions, based on information contained in the Ingenuity Pathways Knowledge Base.

2.4. *Construction of GH1-Tg amago salmon*

Production of GH1 transgenic amago salmon was performed as previously described [23]. Both homozygous (homo) and heterozygous (hetero) amago salmons were derived from a single O. *masou* founder that expressed the gene construct (OnMTGH1). The construct itself comprised of the MT-B promoter from sockeye salmon (*Oncorhynchus nerka*) fused to the coding region of their type 1 GH gene. Non-Tg and GH1-Tg (both homo and hetero) were siblings. After ice anesthesia, their body weight was measured, and pituitary and blood from the caudal vasculature were collected. Blood was kept on ice followed by centrifugation at 750 g for 15 min to obtain plasma samples, which were stored at −80 °C until assayed for measurement of GH1, Insulin-like growth factor I (IGF-I) and lipid metabolites. Meanwhile, the collected pituitaries were used for transcriptome analysis as described below.

2.5. *Measurement of GH1, IGF-I, and lipid metabolites in plasma*

Plasma samples were extracted according to the method of Shimizu et al. (2000) [24]. Levels of GH1 and IGF-I in plasma were measured by homologous radioimmunoassays (RIAs) according to the methods of Swanson (1994) [25] and Moriyama et al. (1994) [26] with slight modifications. Radioactivity of anti-GH1 or anti-IGF-I antibody-bound hormone complexes, which were precipitated with 100 ml of 0.25% PANSORBIN Cells (Calbiochem, Darmstadt, Germany) suspended in RIA buffer, was counted using a Packard COBRA gamma counter (GMI, Ramsey, MN, USA). The lowest detectable levels of GH1 and IGF-I were 0.75 ng/ml and 1.78 ng/ml, respectively. Intra-assay coefficient of variation was less than 5%. Cholesterol and triglyceride concentrations in the serum were determined using a Fuji DRI-CHAM Auto-5 automated analyzer system (Fuji Film, Tokyo, Japan).

2.6. *Quantitative real-time PCR*

Quantitative real-time PCR was performed according to the manufacturer's instructions. Total RNA was extracted from pituitary of GH1-Tg and non-Tg amago salmon using an RNeasy Micro kit (Qiagen, Duesseldorf, Germany). cDNA, from total RNA (1 μg), was synthesized using a Prime Script RT reagent Kit (TAKARA Bio, Shiga, Japan) with oligo dT_{20} random 6-mer primers . Quantitative real-time PCR (qRT-PCR) was performed on a Mx3000P Real-Time QPCR System (Agilent Technologies, Santa Clara, CA, USA) using SYBR Premix Ex Taq II (TAKARA Bio). The mRNA levels of GH1 genes were determined using the $2^{-\Delta\Delta C}$T comparative method. The 18S rRNA was used as the reference genes. Primer sequences are listed in Table 1.

2.7. *Transcriptome analysis using amago salmon-specific subtractive microarray*

To produce an amago salmon-specific subtractive microarray, we constructed subtractive cDNA libraries from 1 μg total RNA from GH1-Tg and non-Tg pituitary, using PCR-Select cDNA Subtraction Kits (Clontech, Mountain View, CA, USA) combined with the SMART PCR cDNA Synthesis kit (Clontech). Differentially expressed cDNA clones were randomly picked and sequenced using BigDye Terminator v3.1/1.1 Cycle Sequencing kits (Applied Biosystems, Foster City, CA, USA), and then identified using the NCBI BLASTN program. cDNA from 1915 independent clones was amplified by PCR, using primers flanking the cloning site (unpublished information). These DNAs, as well as external positive and negative control DNAs, were spotted onto glass microarray slides in triplicate (5760 spots). Aminoallyl-labeled antisense RNA microarray probes were synthesized from GH1-Tg or non-Tg total RNAs (1 μg) using the MessageAmpII aRNA Amplification Kit (Ambion, Foster City, CA, USA). These RNA probes (8 μg) were

Table 1 – Primer list for RT-PCR analysis.

(1) GH1 common primers
Forward: 5′-CTGATGAACGCAGACAGC-3′
Reverse: 5′-CCAGGATTCAATCAGACGG-3′
(2) GH1 transgene-specific primers (transgene is from sockeye salmon)
Forward: 5′-AATTCTCCCAGCGTCGTTAG-3′
Reverse: 5′-CCAGGATTCAATCAGACGG-3′
(3) Amago-specific primers
Forward: 5′-GATATTCCTGCTGGACTTC-3′
Reverse: 5′-GATGGTTTTACTTGCAATGATTGTG-3′
(3) 18S rRNA (control) primers
Forward: 5′-GGTGGAGCGATTTGTCTGG-3′
Reverse: 5′-CTCAATCTCGTGTGGCTGAAC-3′

coupled with Cy5 or Cy3 dye. Microarray analysis, which included dye-swap experiments to compensate for dye-specific labeling effect, was repeated by using five independently generated salmon probes. Detailed protocols for hybridization, signal scanning and microarray processing have been described in a previous report [23,27].

Background signals were subtracted from the raw data, and the data were then subjected to Lowess normalization (locally weighted scatter plot smoothing) between the Cy5 and Cy3 channels. Signal intensities under 1000 were eliminated. The average signal intensities of Cy5 and Cy3 were obtained, and the dye-swap log ratios (GH1-Tg/non-Tg) were calculated as the logarithm of the ratios of the Cy5 and Cy3 intensities. These transformed dye-swap log ratios were analyzed using an unpaired Student's t-test (fold change >1.5, $p<0.05$ corrected by Benjamini–Hochberg FDR) using the Avadis 4.3 software (Strand Inc., Bangalore, India).

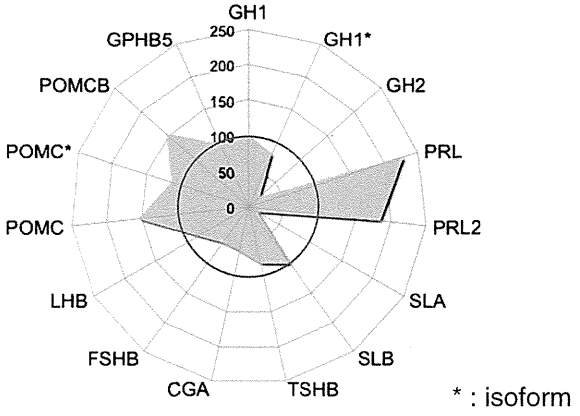

Fig. 2 – Expression levels of pituitary hormones affected by excess GH1 treatment. The green chart indicates the levels of pituitary hormones expressed at different levels in the excess GH1-treated vs. non-treated pituitary. Red circle indicates expression levels of pituitary hormones in non-treated pituitary. Asterisks indicate isoforms of identical pituitary hormone.

3. Results and discussion

3.1. *Protein profile in salmon pituitary treated with GH1*

In order to identify pituitary proteins that specifically increase or decrease in response to excess GH1, we performed comprehensive and quantitative proteome analysis using iTRAQ

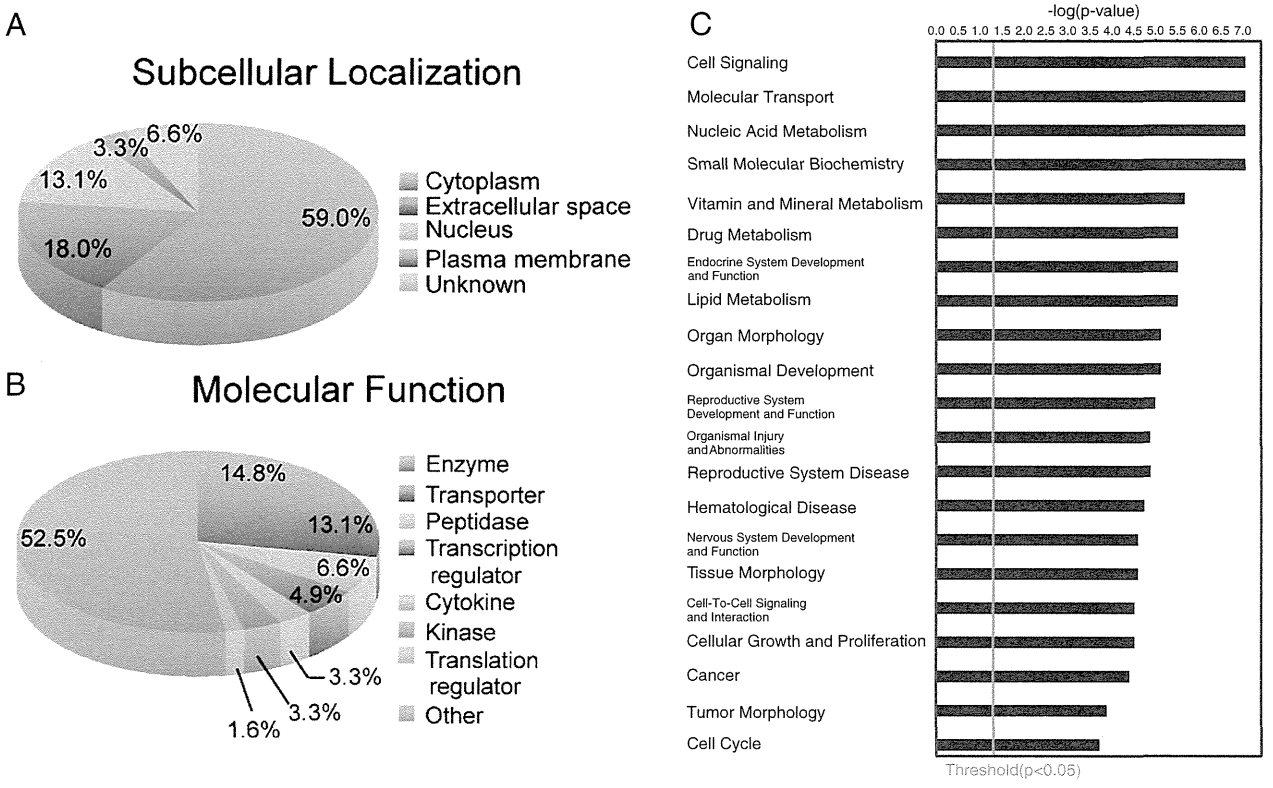

Fig. 1 – Functional classification of pituitary proteins differentially expressed in response to excess GH1 treatment. (A) Subcellular localization of proteins differentially expressed in the excess GH1-treated pituitary compared to non-treated pituitary. Sixty-one proteins with human homologs were classified into each annotation category by the Ingenuity Pathways Knowledge Base. (B) Molecular functions of the differentially expressed proteins described in Fig. 1A. (C) Biological functions associated with 61 homologous human proteins, obtained from the Ingenuity Pathways Knowledge Base. Fisher's exact test was used to calculate a p-value (threshold $p<0.05$) for each biological function.